PERGAMON

International Journal of Solids and Structures 36 (1999) 2973–3013

INTERNATIONAL JOURNAL OF SOLIDS and STRUCTURES

A closed-form solution procedure for circular cylindrical shell vibrations[1]

Joseph Callahan[2], Haim Baruh*

Department of Mechanical and Aerospace Engineering, Rutgers University, Piscataway, NJ 08855-0909, U.S.A.

Received 3 September 1996; in revised form 16 March 1998

Abstract

A systematic procedure for obtaining the closed-form eigensolution for thin circular cylindrical shell vibrations is presented, which utilizes the computational power of existing commercial software packages. For cylindrical shells, the longitudinal, radial, and circumferential displacements are all coupled with each other due to Poisson's ratio and the curvature of the shell. For beam and plate vibrations, the eigensolution can often be found without knowledge of absolute dimensions or material properties. For cylindrical shell vibrations, however, one must know the relative ratios between shell radius, length, and thickness, as well as Poisson's ratio of the material. The mode shapes and natural frequencies can be determined analytically to within numerically determined coefficients for a wide variety of boundary conditions, including elastic and rigid ring stiffeners at the boundaries. Excellent agreement is obtained when the computed natural frequencies are compared with known experimental results.

1. Introduction

Of all existing shell models, the circular cylindrical shell is perhaps the most widely studied. It has applications in chimney design, pipe flow, and aircraft fuselages to name a few. Many shell theories have been developed over the last century, as well as methods to solve their governing equations. A comprehensive review and comparison of shell theories has been done by Leissa (1973). Here we will restrict the solution to the set of thin shell equations derived by Junger and Feit (1972). For static analysis, various methods of solution have been proposed. Vinson (1974) used an operator approach and manipulated the governing equations to obtain a single equation for the radial deformation. The circumferential and longitudinal displacements are then determined

* Corresponding author. Fax: 001 908 445 5313; E-mail: baruh@jove.rutgers.edu; WWW: http://www-srac.rutgers.edu/~baruh

[1] Supported by the Federal Aviation Administration.

[2] E-mail: jcallaha@jove.rutgers.edu; WWW: http://www.rci-rutgers.edu/~jcallaha

0020–7683/99/$ - see front matter
PII: S0020–7683(98)00139–5

by back substitution using the radial solution. Niordson (1985) also took an operator approach but showed that the deflections can all be derived from a potential function.

The vibration problem for a general shell element has been formulated by Soedel (1981) using Hamilton's principle. The presence of second time derivatives makes the approaches used in the static case very cumbersome due to the increase in the number of terms. Junger and Feit (1972) assumed displacements of a certain form, determined the boundary conditions that they satisfy, and restricted discussion to that case. Niordson (1985) used a similar approach in his treatment of cylindrical shell vibrations, with both sets of authors dealing with freely-supported end conditions. While this approach produces three frequencies corresponding to the three principal motions for each model configuration, they are not obtained in increasing numerical order. When scanning through a desired frequency band, some modes may be inadvertently overlooked.

In this work, the method presented matches individual modes to individual frequencies for any set of boundary conditions. In this manner, for each modal arrangement there exists a single frequency and a single correspondence between the radial, longitudinal, and circumferential displacements. This is the approach outlined by Love (1944) but not pursued in its complete form due to its mathematical complexity. With the advent of high performance computers, however, the intense calculations required by such an approach are now possible. In the present procedure, the circumferential and longitudinal displacements are scaled off of the radial deformation, as done by others (see e.g. Forsberg, 1964; Warburton, 1965; Leissa, 1973; Soedel, 1981). Chung (1981) developed a procedure to obtain the solution of Sanders' shell equations for various boundary conditions by representing the axial behavior of the modal displacements as Fourier series expansions, obtaining an explicit frequency equation in the form of an infinite series. Ludwig and Krieg (1981) presented a method to obtain the eigensolution of Flügge's equations by transforming them into algebraic equations in terms of constants to be evaluated numerically. Approximations were only made in the root solving algorithm for the frequency determinant; the reduction of the partial differential equations of motion to an algebraic system was exact. For both of these methods, the natural frequencies can be determined to a high degree of accuracy. They give analytical solutions to the associated equations of motion for their respective shell theories, but do not discuss modal orthogonality. The shell theories of Flügge and Sanders can both be shown to lead to orthogonal modes, but this is often assumed without proof.

In order to apply modal analysis and control, it is also desirable to ensure that the equations of motion were derived consistently with the associated boundary conditions. In this manner, the natural mode shapes will form a set of orthogonal basis functions. For forced vibration response, this reduces the three partial differential equations of motion to a set of ordinary oscillator equations. Bogner and Archer (1965) showed that for clamped, simply-supported, and free end conditions, the axisymmetric modes of a general shell of revolution are orthogonal. Tso (1967) used Hamilton's principle to show that the modes are orthogonal if the displacements or their corresponding natural forces vanish on the shell boundaries. For a general shell element, Soedel (1981) showed that the mode shapes will be mutually orthogonal when the boundary conditions are conservative. In this paper, we show modal orthogonality by integrating the stiffness operator of the system by parts, as done by Meirovitch (1967) for beams and plates.

The solutions of the equations of motion derived by Junger and Feit (1972), which follow directly from Soedel's formulation (1981) when tailored to a cylindrical shell, will lead to orthogonal modes because the natural boundary conditions are derived consistently with the governing equations of

motion. Although the choice of boundary conditions has a significant effect on the shape of the natural modes (see e.g. Forsberg, 1964; Koga, 1988), orthogonality can be guaranteed for a large variety of boundary conditions before the eigensolution is attempted. In addition to the classical free and fixed boundary condition combinations used in the literature, we also investigate the effect of replacing a free end with an elastic ring stiffener. The elastic strain and kinetic strain energies derived by Galletly (1955) will be modified according to Al-Najafi and Warburton (1970) to be consistent with the coordinate system used in this analysis. Qualitatively, many boundary conditions can be recovered from the elastic ring when certain parameters are permitted to take on extreme values. Letting the elastic modulus go to infinity leads to a rigid ring, while letting it and the mass density go to zero will produce a free end.

Extensive experimental data has also been generated for cylindrical shells in recent years. The frequencies obtained from Junger and Feit's equations of motion agree very well with experimental data for clamped–clamped (from Arnold and Warburton, 1953; Koval and Cranch, 1962), freely supported–freely supported (from Bert et al., 1969; Bray and Egle 1970), and clamped–free (from Gill, 1972; Sharma and Johns, 1972; Khaddakar et al., 1988; Raj et al., 1995) boundary conditions. The procedure presented here can also accurately predict vibration frequencies for elastic ring–elastic ring end conditions (from Brogan et al., 1968; El Raheb and Babcock, 1981).

The overall motivation was to develop a self-contained, systematic, and analytical procedure to generate orthogonal eigensolutions for any given set of boundary conditions taking full advantage of the computational power of the software packages MATLAB by the MathWorks, Inc. and MAPLE V by Waterloo Maple Software. Once we have the eigensolution, regardless of the shell theory, modal analysis techniques are applicable. Forced response can be readily obtained as time dependent linear combinations of the natural modes. Expressions for the modal displacements are exact to within numerically determined coefficients. The advantage of explicit displacements over finite element solutions is the absence of numerical error often introduced when derivatives are computed from finite difference approximations. Higher modes are calculated with the same accuracy as lower modes. Modal control is also possible when accurate estimation of the system behavior can be ascertained. Another advantage of the current approach over finite element methods is that all modal information can be generated within and stored by the commercial code MATLAB without a large memory requirement. Depending on the mesh size used, finite element packages can have several orders of magnitude more bits of information on a particular modal layout than the analytical approach here. Large displacement gradients that often exist near the shell boundaries can also be captured without a decrease in spatial mesh size. Once an eigensolution library is obtained, simulations of forced response and modal control can be accomplished within MATLAB as well, calling the required modal parameters as needed. No interface between eigensolution information and shell simulation needs to be developed. The tool developed here makes feasible eigensolution sensitivity studies by simply redefining shell parameters and boundary condition combinations. Most important, the methodology presented in this paper is not limited to the shell theory discussed herein.

2. Equations of motion

A cylindrical shell element is shown in Fig. 1, where a, h, and l are the respective shell radius, thickness, and length. Here the respective displacements in the z-, θ-, and r-directions are denoted

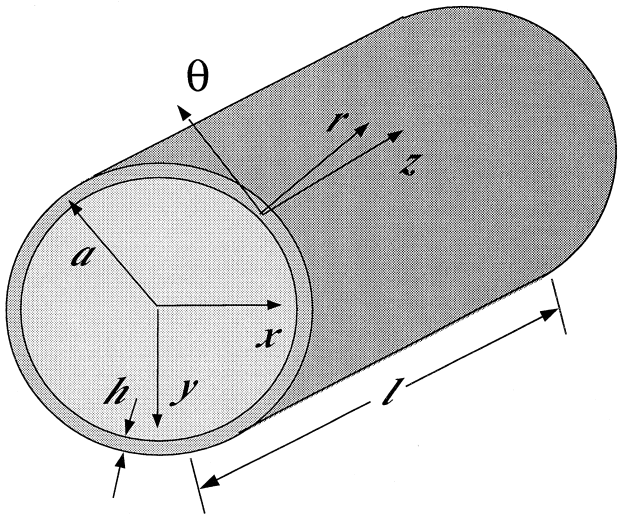

Fig. 1. A circular cylindrical shell element.

by u, v, and w. Relevant material properties are the Young's modulus E, mass density ρ, and Poisson's ratio v. If the primary shell displacements are arranged into a vector according to

$$\mathscr{U}(z,\theta,t) = \{u(z,\theta,t) \quad v(z,\theta,t) \quad w(z,\theta,t)\}^T \tag{1}$$

then the governing equations can be expressed in standard operator notation as:

$$L[\mathscr{U}(z,\theta,t)] + \mathscr{M}\frac{\partial^2 \mathscr{U}(z,\theta,t)}{\partial t^2} = \mathscr{F}(z,\theta,t) \tag{2}$$

where L and $\mathscr{M}$ are the 3×3 stiffness and inertial operators and $\mathscr{F}$ is the external traction vector containing the distributed loads applied in the longitudinal, circumferential, and radial directions. For this analysis we will use the equations of motion derived by Junger and Feit (1972), which follow directly from Soedel's formulation (1981) when tailored to a thin cylindrical shell. For this case, the operators have the form:

$$L = -\frac{Eh}{1-v^2}\begin{bmatrix} L_{11} & L_{12} & L_{13} \\ L_{12} & L_{22} & L_{23} \\ -L_{13} & -L_{23} & L_{33} \end{bmatrix} \tag{3}$$

$$L_{11} = \frac{\partial^2}{\partial z^2} + \frac{1-v}{2a^2}\frac{\partial^2}{\partial \theta^2}, \quad L_{12} = \frac{1+v}{2a}\frac{\partial^2}{\partial z\,\partial \theta}$$

$$L_{13} = \frac{v}{a}\frac{\partial}{\partial z}, \quad L_{22} = (1+\beta^2)\left(\frac{1-v}{2}\frac{\partial^2}{\partial z^2} + \frac{1}{a^2}\frac{\partial^2}{\partial \theta^2}\right)$$

$$L_{23} = \left[\frac{1}{a^2} - \beta^2\left(\frac{\partial^2}{\partial z^2} + \frac{1}{a^2}\frac{\partial^2}{\partial \theta^2}\right)\right]\frac{\partial}{\partial \theta}, \quad L_{33} = -\frac{1}{a^2} - \beta^2\left(a\frac{\partial^2}{\partial z^2} + \frac{1}{a}\frac{\partial^2}{\partial \theta^2}\right)^2$$

$$\mathscr{M} = \rho h[I_{3\times 3}] \tag{4}$$

where $\beta^2 = h^2/12a^2$.

3. Solution procedure

As done for most continuous systems, the first attempt in solving these equations is the assumption that the response is separable in space and time. Applying a modal expansion of the form

$$\mathscr{U}(z,\theta,t) = \sum_{k=1}^{\infty} \mathscr{U}_k(z,\theta)\eta_k(t) \tag{5}$$

leads to a harmonic time dependence, with each mode vibrating at a frequency ω_k. Here, $\eta_k(t)$ is the scalar modal coordinate corresponding to the mode $\mathscr{U}_k(z,\theta)$. For free vibration ($\mathscr{F} = \{0\}$), this leads to the standard eigenvalue problem:

$$L\{\mathscr{U}_k(z,\theta)\} = \omega_k^2 \mathscr{M}\{\mathscr{U}_k(z,\theta)\} \tag{6}$$

The next step is to separate the spatial dependence of the solution between the axial and circumferential directions. For a closed shell, the modal displacements are assumed to be harmonic in the θ-direction, given by

$$\{u(z,\theta) \quad v(z,\theta) \quad w(z,\theta)\}^T = \{U(z)\sin n\theta \quad V(z)\cos n\theta \quad W(z)\sin n\theta\}^T \tag{7}$$

where n is an integer. The harmonic θ-dependence results from requiring the continuity of the shell displacements along the tangential direction. Due to circular symmetry, all modes other than the axisymmetric case will be two-fold degenerate, as the assumed displacements

$$\{u(z,\theta) \quad v(z,\theta) \quad w(z,\theta)\}^T = \{U(z)\cos n\theta \quad -V(z)\sin n\theta \quad W(z)\cos n\theta\}^T \tag{8}$$

will also produce the same equations of motion and thus yield the same eigensolution.

Now that both the time and θ-contributions have been factored out of the response, what remains is to determine the z-dependence of the modal displacements. At this point, we can manipulate the equations of motion to obtain a single equation describing the radial deflection. Once this is done, the remaining displacements can be found by back substitution. This was the approach taken by Vinson (1974) and is effectively a Gaussian elimination applied to the stiffness. This technique works well for static shell analysis because the right hand side of eqn (6) vanishes for the static case. The problem with this approach for the dynamic case is the large amount of terms that result.

Dealing with the equations of motion in their present form, Love (1944) proposed that modal displacements share the same exponential behavior multiplied by different constants. Since we now have three ordinary differential equations in the z variable, this is the standard way to proceed. Although he obtained a different set of governing shell equations, we will use a similar procedure

to solve eqn (2). In fact, the solution approach outlined here can be extended to most sets of linear shell equations, including those for orthotropic shells or specially orthotropic laminates. In Love's approach, the constant for the longitudinal displacement can be chosen arbitrarily, but the other two are some multiples of this value. These multiples determine the ratios between the three modal deflections. It was determined after some preliminary research that choosing the constant for the radial displacement as arbitrary was a better choice because it tends to dominate the motion at higher circumferential mode numbers. In a slight modification of Love's approach, the modal deflections are assumed to have the following form:

$$\{U(z) \quad V(z) \quad W(z)\}^T = A\,\mathrm{e}^{\alpha_m z/a}\{C \quad B \quad 1\}^T \tag{9}$$

where α, A, B, and C are constants (for a given frequency) to be determined. By factoring A out of the modal response and treating B and C as scaling factors, their values can be determined based on the modal frequency and system parameters only, while still capturing the ratio between the modal displacements. This scaling has been done by many authors over the years (see e.g. Forsberg, 1964; Warburton, 1965; Leissa, 1973; Soedel, 1981), as the radial motion is usually the dominant feature at lower bandwidths. Here, the values of α_m are given in subscript to show that they are directly related to the axial modal number m for a fixed tangential mode number n. To avoid confusion with other summation indices, however, it will be dropped in future discussion. The dependence of the modal frequencies on the integer mode numbers m and n will be addressed later in some parametric studies. Following standard procedure, defining a non-dimensional frequency parameter $\Omega^2 = \omega^2\rho a^2(1-\nu^2)/E$, and substituting eqn (9) into the eigenvalue problem leads to

$$\begin{bmatrix} \Omega^2+\alpha^2-\frac{1-\nu}{2}n^2 & -\frac{1+\nu}{2}n\alpha & \nu\alpha \\ \frac{1+\nu}{2}n\alpha & \Omega^2+(1+\beta^2)\left(\frac{1-\nu}{2}\alpha^2-n^2\right) & n[1+\beta^2(n^2-\alpha^2)] \\ -\nu\alpha & n[1+\beta^2(n^2-\alpha^2)] & \Omega^2-\beta^2[\alpha^2-n^2]^2-1 \end{bmatrix} \begin{bmatrix} C \\ B \\ 1 \end{bmatrix} = \begin{bmatrix} 0 \\ 0 \\ 0 \end{bmatrix} \tag{10}$$

For a non-trivial solution of the equations of motion, the determinant of this coefficient matrix must vanish for each value of n. This leads to an eighth-order polynomial in α whose roots determine the z-dependence of the mode shapes. In general, solving the roots of the determinant of eqn (10) for α is not possible in closed form. Hence, people have often resorted to approximate techniques at this point. We took advantage of computer software packages to carry the original determinant through the analysis and have them compute the numerical values once the shell ratios are specified.

As observed by Love (1944), it can be shown that no odd powers appear in the determinant of the matrix in (10), making it a fourth-order polynomial in α^2. Therefore, the general solution for the modal displacements can be written in its final form as

$$U(z) = \sum_{r=1}^{4} C_r\{A_r\,\mathrm{e}^{\alpha_r z/a} - A'_r\,\mathrm{e}^{-\alpha_r z/a}\} \tag{11}$$

$$V(z) = \sum_{r=1}^{4} B_r \{A_r \, e^{\alpha_r z/a} + A'_r \, e^{-\alpha_r z/a}\} \tag{12}$$

$$W(z) = \sum_{r=1}^{4} \{A_r \, e^{\alpha_r z/a} + A'_r \, e^{-\alpha_r z/a}\} \tag{13}$$

where the constants B_r and C_r are determined by solving any two of the three equations in the matrix expression (10). The negative sign appears in the summations for the longitudinal displacement because C_r can be shown to be odd in α_r. The expressions for B_r, C_r, and α_r are as yet independent of the boundary conditions prescribed at $z = 0$ and $z = l$. For a given value of h/a, l/a, and v, these parameters are functions of the non-dimensional frequency Ω only. The form of the solution in (11)–(13) has been known for some time but most researchers have resorted to finite element solutions due to the effort required to solve for the coefficients. Solving the eigenvalue problem for a cylindrical shell is often called an inverse approach in the sense that the frequency can be specified, from which the associated values of α follow. Thus, one can find the shell length for a given frequency. Modern software packages make it possible to do this quickly in an iterative fashion, making is possible to vary the frequency value until the appropriate length parameters α have been found. The primary effort in this analysis is to automate the procedure using the software packages MAPLE and MATLAB to generate the required expressions and iterate through a natural frequency band to find all associated zeros of the frequency equation. At this point, one could also investigate the nature of the roots α_r in order to express the displacements (11)–(13) in terms of strictly real numbers. During the research for this study, we found that two of the four roots usually appeared as complex conjugate pairs, while the other two were either real or imaginary but uncorrelated. While finding the coefficients numerically, no pattern was found for the behavior of the roots, so we chose to leave the displacements in the compact form given above. Further investigation may show purely real expressions for the modal displacements, but they would be undoubtedly very lengthy. We outline the numerical solution for the roots α_r in Section 6.

For the axisymmetric modes, the assumed modal displacements have the simpler form:

$$\{u(z,\theta) \quad v(z,\theta) \quad w(z,\theta)\}^T = \{U(z) \quad V(z) \quad W(z)\}^T \tag{14}$$

Since there is no θ-dependence for this class of modes, the natural frequencies will be distinct. With n set to zero, the determinant of the coefficient matrix in (10) set to zero leads to the following characteristic equation:

$$\left[(1+\beta^2)\frac{1-v}{2}\alpha^2 + \Omega^2\right][(\alpha^2+\Omega^2)(\beta^2\alpha^4 + 1 - \Omega^2) - v^2\alpha^2] = 0 \tag{15}$$

Here, the torsional motion decouples from the radial and longitudinal vibrations. Defining the root for this case as $\alpha_1^2 = -2\Omega^2/(1-v)(1+\beta^2)$, the axisymmetric torsional modes have the form

$$U(z) = W(z) = 0, \quad V(z) = A_1 \cos\gamma\frac{z}{a} + A'_1 \sin\gamma\frac{z}{a} \tag{16}$$

where $\gamma = \Omega\sqrt{2/(1-v)(1+\beta^2)}$. When this result of Junger and Feit's theory is compared with that of torsional shaft vibration, the only difference is the appearance of the $(1+\beta^2)$ term. This occurs

because the circumferential deflection v has a small contribution to the bending strains. The axisymmetric torsional modes can also be obtained by setting $n = 0$ in eqn (7).

The other class of axisymmetric vibrations consists of longitudinal motion coupled with radial displacement, characterized by the remaining three roots α_r^2 $(r = 2, 3, 4)$ with the general form:

$$U(z) = \sum_{r=2}^{4} \frac{\nu\alpha_r}{\Omega^2 + \alpha_r^2} \{A_r' \, \mathrm{e}^{-\alpha_r z/a} - A_r \, \mathrm{e}^{\alpha_r z/a}\} \tag{17}$$

$$V(z) = 0 \tag{18}$$

$$W(z) = \sum_{r=2}^{4} \{A_r \, \mathrm{e}^{\alpha_r z/a} + A_r' \, \mathrm{e}^{-\alpha_r z/a}\} \tag{19}$$

These can be found by setting $n = 0$ in eqn (8). As discussed for the general case, the frequency equation and relations between constants are determined by the boundary conditions. Since torsion decouples from the other vibration types, the two classes can be normalized separately. Both types will appear in the frequency spectrum, however, so the axisymmetric torsional frequencies must be included when predicting modes within a given frequency band.

The rigid body modes can be found by setting the frequency to zero in the equations of motion and solving for modes that have zero mid-plane strain. Table 1 gives the general forms of the rigid body modes, where $\mathscr{C}$ is an arbitrary constant. Due to the two-fold degeneracy of the bending modes ($n = 1$), we have a total six rigid body modes. This is consistent with intuition, since a rigid body in space has six degrees of freedom, three in translation plus three in rotation.

4. Boundary conditions

At each end of the cylindrical shell, four boundary conditions must be specified. Constraints can be placed on the geometric boundary conditions $U(z)$, $V(z)$, $W(z)$, and $\mathrm{d}W(z)/\mathrm{d}z$, their associated internal loads, or some combination of them. When the extended Hamilton's principle is applied, one obtains the equations of motion within the shell domain as well as boundary expressions. Denoting U and T as the respective elastic strain and kinetic energies, applying this variational technique yields

Table 1
Rigid body modes for the circular cylindrical shell

Mode type	n	$u(z, \theta)$	$v(z, \theta)$	$w(z, \theta)$
Translation z-direction	0	$\mathscr{C}$	0	0
Rotation z-axis	0	0	$\mathscr{C}$	0
Translation y-direction	1	0	$\mathscr{C}\cos\theta$	$\mathscr{C}\sin\theta$
Rotation x-axis	1	$\mathscr{C}\sin\theta$	$-\mathscr{C}(z/a)\cos\theta$	$-\mathscr{C}(z/a)\sin\theta$
Translation x-direction	1	0	$-\mathscr{C}\sin\theta$	$\mathscr{C}\cos\theta$
Rotation y-axis	1	$\mathscr{C}\cos\theta$	$\mathscr{C}(z/a)\sin\theta$	$-\mathscr{C}(z/a)\cos\theta$

$$\int_{t_1}^{t_2} \delta(T-U+\mathscr{W})\,\mathrm{d}t = -\int_{t_1}^{t_2}\int_0^{2\pi}\int_0^{l} \delta\mathscr{U}^T\left\{\mathscr{M}\frac{\partial^2\mathscr{U}}{\partial t^2}+L[\mathscr{U}]-\mathscr{F}\right\}a\,\mathrm{d}\theta\,\mathrm{d}z\,\mathrm{d}t$$
$$-\int_{t_1}^{t_2}\int_0^{2\pi}\left[N_z\delta u+S_z\delta v+V_z\delta w-M_z\delta\left(\frac{\partial w}{\partial z}\right)\right]_{z=0}^{z=l} a\,\mathrm{d}\theta\,\mathrm{d}t \quad (20)$$

where $\mathscr{W}$ is the external work done by the force vector $\mathscr{F}$ and the internal forces along constant z-section are related to the shell displacements (following Soedel's 1981 procedure) according to

$$M_z(z,\theta) = -\frac{Eh^3}{12(1-\nu^2)}\left\{\frac{\partial^2 w}{\partial z^2}+\frac{\nu}{a^2}\left(\frac{\partial^2 w}{\partial\theta^2}-\frac{\partial v}{\partial\theta}\right)\right\} \quad (21)$$

$$V_z(z,\theta) = -\frac{Eh^3}{12(1-\nu^2)}\left\{\frac{\partial^3 w}{\partial z^3}+\frac{1}{a^2}\left[(2-\nu)\frac{\partial^3 w}{\partial z\,\partial\theta^2}-\frac{\partial^2 v}{\partial z\,\partial\theta}\right]\right\} \quad (22)$$

$$N_z(z,\theta) = \frac{Eh}{1-\nu^2}\left\{\frac{\partial u}{\partial z}+\frac{\nu}{a}\left(\frac{\partial v}{\partial\theta}+w\right)\right\} \quad (23)$$

$$S_z(z,\theta) = \frac{Eh}{2(1+\nu)}\left\{\frac{1}{a}\frac{\partial u}{\partial\theta}+(1+\beta^2)\frac{\partial v}{\partial z}-2\beta^2\frac{\partial^2 w}{\partial z\,\partial\theta}\right\} \quad (24)$$

where M_z is the internal bending moment, V_z is the transverse shear force, N_z is the membrane normal force, and S_z is the membrane shear force. These quantities are defined to be positive in the directions indicated in Fig. 2. Here, t_1 and t_2 are the endpoints of an arbitrary time interval, at which the variations (denoted by the δ-operation) of the shell displacements are required to vanish. The displacement vectors (7) or (8) may be substituted into these expressions to yield the internal forces for any given circumferential mode number n.

At each end ($z = 0$ and $z = l$) four conditions must be specified. Substituting the general forms of the modal displacements into these constraints lead to the following expression

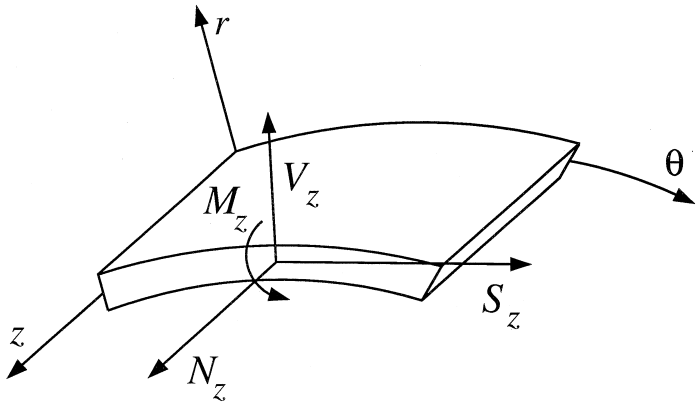

Fig. 2. Internal forces at a constant z section on the cylindrical shell.

Table 2
Coefficient matrix Q entries for the non-axisymmetric modes ($n > 0$) subject to different boundary conditions

	$(r = 1, \ldots, 4)$	
End condition	$Q_{*,r}$	$Q_{*,r+4}$
$V(\Delta a) = 0$	$B_r e^{\alpha_r \Delta}$	$B_r e^{-\alpha_r \Delta}$
$U(\Delta a) = 0$	$C_r e^{\alpha_r \Delta}$	$-C_r e^{-\alpha_r \Delta}$
$W(\Delta a) = 0$	$e^{\alpha_r \Delta}$	$e^{-\alpha_r \Delta}$
$W'(\Delta a) = 0$	$\alpha_r e^{\alpha_r \Delta}$	$-\alpha_r e^{-\alpha_r \Delta}$
$S_z(\Delta a) = 0$	$[nC_r + \alpha_r B_r(1+\beta^2) - 2\beta^2 n\alpha_r] e^{\alpha_r \Delta}$	$-[nC_r + \alpha_r B_r(1+\beta^2) - 2\beta^2 n\alpha_r] e^{-\alpha_r \Delta}$
$N_z(\Delta a) = 0$	$[C_r\alpha_r + v(1 - nB_r)] e^{\alpha_r \Delta}$	$[C_r\alpha_r + v(1 - nB_r)] e^{-\alpha_r \Delta}$
$V_z(\Delta a) = 0$	$\alpha_r[\alpha_r^2 + nB_r - (2-v)n^2] e^{\alpha_r \Delta}$	$-\alpha_r[\alpha_r^2 + nB_r - (2-v)n^2] e^{-\alpha_r \Delta}$
$M_z(\Delta a) = 0$	$[\alpha_r^2 + vn(B_r - n)] e^{\alpha_r \Delta}$	$[\alpha_r^2 + vn(B_r - n)] e^{-\alpha_r \Delta}$

$$[Q] \begin{Bmatrix} A \\ A' \end{Bmatrix} = \{0\} \tag{25}$$

where Q is an 8×8 coefficient matrix whose rows depend on the boundary conditions. For a non-trivial solution, the determinant of this coefficient matrix set to zero is the frequency equation for the shell modes with circumferential mode number $n > 0$. When any of the natural boundary conditions upon application of (21)–(24) are required to vanish, it must do so regardless of θ, forcing the z-dependent portion to vanish. Table 2 shows the matrix entries for various boundary conditions prescribed at $z = \Delta a$. Entries at $z = 0$ are found by setting Δ to zero, and those at the end $z = l$ by setting Δ to l/a.

For the axisymmetric case, all derivatives with respect to θ vanish. In this case, the torsional mode decouples, rendering the matrix Q given in eqn (25) block diagonal. Thus, it can be dealt with independent of the radial and longitudinal motion. This results in two independent matrix equations: one involving a 2×2 coefficient matrix for the torsion problem and the second involving a 6×6 coefficient matrix corresponding to the other modes. The product of the determinants of these two coefficient matrices set to zero is the frequency equation for the axisymmetric modes. The Q matrix entries of the axisymmetric case can be deduced from Table 2 by setting $n = 0$.

Another boundary condition we consider here is the stiffening effect of an elastic ring. The analysis for this case begins with elastic strain and kinetic energy expressions similar to those derived by Galletly (1955) but modified according to Al-Najafi and Warburton (1970) to be consistent with the coordinate system used in Fig. 1. As done in these analyses, the cross-sectional dimensions of the ring are assumed to be small relative to the ring radius, resulting in a shallow ring theory. For a ring stiffener located at $z = z_R$, the elastic strain energy can be expressed in terms of the local ring displacements by:

$$U_R = \frac{1}{2} \int_0^{2\pi} \left[\frac{E_R I_G^r}{a_R^2} \left(\frac{1}{a_R} \frac{\partial^2 u_R}{\partial \theta^2} - \frac{\partial w_R}{\partial z} \right)^2 + \frac{E_R I_G^z}{a_R^4} \left(\frac{\partial^2 w_R}{\partial \theta^2} + w_R \right)^2 \right.$$

$$+\frac{E_R A_R}{a_R^2}\left(w_R+\frac{\partial v_R}{\partial\theta}\right)^2+\frac{G_R C_T}{a_R^2}\left(\frac{\partial^2 w_R}{\partial z\,\partial\theta}+\frac{1}{a_R}\frac{\partial u_R}{\partial\theta}\right)^2\Bigg]_{z=z_R} a_R\,\mathrm{d}\theta \quad (26)$$

where the subscript R denotes quantities measured relative to the centerline of the ring. Here, E_R and G_R are the respective Young's and shear moduli of the ring. The quantities I_G^r and I_G^z are the area moments of inertia of the ring cross-section about the r- and z-directions. The cross-sectional area and St Venant torsional constant are denoted by A_R and C_T, respectively. Each term in eqn (26) corresponds to a different type of deformation. The first two are due to bending about the longitudinal and radial directions, the third accounts for extension of the ring in the circumferential direction, while the fourth and final term is the torsional contribution. Although one is not limited to a particular ring cross-section, the effects of warping are not included in eqn (26).

The kinetic energy of the ring stiffener, including rotatory inertia, can be expressed by:

$$T_R=\frac{1}{2}\rho_R\int_0^{2\pi}\left[A_R(\dot{u}_R^2+\dot{v}_R^2+\dot{w}_R^2)+I_G^\theta\left(\frac{\partial\dot{w}_R}{\partial z}\right)^2+\frac{I_G^z}{a^2}\left(\frac{\partial\dot{w}_R}{\partial\theta}\right)^2\right]_{z=z_R} a_R\,\mathrm{d}\theta \quad (27)$$

where ρ_R and I_G^θ are the respective mass density and area moment of inertia of the ring cross-section about the θ-direction.

In general, the centroid of the ring cross-section may not coincide with a desired circumference on the shell. To account for this, one can permit both a radial offset ea and an axial offset ba, where e and b are fractions of the shell radius, measured positive in their associated coordinate directions. In this general case, the ring deformations can be shown to be related to those of the shell according to:

$$u_R=u-ea\frac{\partial w}{\partial z} \quad (28)$$

$$v_R=(1+e)v-e\frac{\partial}{\partial\theta}\left(w+ba\frac{\partial w}{\partial z}\right) \quad (29)$$

$$w_R=w+ba\frac{\partial w}{\partial z} \quad (30)$$

with $a_R=(1+e)a$. Ring stiffeners with radial eccentricity only can be recovered by setting $b=0$. Elastic rings symmetrically disposed about the shell mid-plane result when $e=0$. For rings attached to the shell somewhere between the shell ends, treating the case $b\neq 0$ is not necessary. For situations in which the shell ends with a stiffener, however, allowing for a longitudinal as well as a radial offset makes it possible to preserve the original length of the undeformed shell, facilitating sensitivity analyses as well. For the general case, eqns (28)–(30) must be substituted into the elastic strain and kinetic energy expressions for the ring. Once this is done, Hamilton's principle must be applied to the total kinetic and strain energy. For a ring located at $z=z_R$, we obtain the same governing dynamic relations for the shell interior, but the variational operation in eqn (20) results in an additional boundary term at the ring location, shown here by:

$$\int_{t_1}^{t_2}\delta(T+T_R-U-U_R+\mathscr{W})\,\mathrm{d}t = -\int_{t_1}^{t_2}\int_0^l\int_0^{2\pi}\delta\mathscr{U}^T\left\{\mathscr{M}\frac{\partial^2\mathscr{U}}{\partial t^2}+L[\mathscr{U}]-\mathscr{F}\right\}a\,\mathrm{d}\theta\,\mathrm{d}z\,\mathrm{d}t$$
$$-\int_{t_1}^{t_2}\int_0^{2\pi}\left[N_z\delta u+S_z\delta v+V_z\delta w-M_z\delta\left(\frac{\partial w}{\partial z}\right)\right]_{z=0}^{z=l}a\,\mathrm{d}\theta\,\mathrm{d}t$$
$$+\int_{t_1}^{t_2}\int_0^{2\pi}\left[N_z^R\delta u+S_z^R\delta v+V_z^R\delta w-M_z^R\delta\left(\frac{\partial w}{\partial z}\right)\right]_{z=z_R}a\,\mathrm{d}\theta\,\mathrm{d}t \tag{31}$$

The negative sign on the shell internal forces is a consequence of their positive orientation defined in Fig. 2. Boundary conditions for the general ring stiffener case with $e \neq b \neq 0$ have been derived by Callahan (1997). For simplicity of analysis, however, the remainder of this section will assume that the centerline of the ring coincides that of the shell terminus (i.e. $e = b = 0$). In this case, the effective internal forces/moment due to the elastic ring can be expressed as:

$$M_z^R(z,\theta) = \frac{E_R I^r}{a^2}\left(\frac{\partial w}{\partial z}-\frac{1}{a}\frac{\partial^2 u}{\partial\theta^2}\right)-\frac{G_R C_T}{a^2}\left(\frac{1}{a}\frac{\partial^2 u}{\partial\theta^2}+\frac{\partial^3 w}{\partial z\,\partial\theta^2}\right)+\rho_R I^\theta\frac{\partial\ddot{w}}{\partial z} \tag{32}$$

$$V_z^R(z,\theta) = -\frac{E_R I^z}{a^4}\left(w+2\frac{\partial^2 w}{\partial\theta^2}+\frac{\partial^4 w}{\partial\theta^4}\right)-\frac{E_R A_R}{a^2}\left(w+\frac{\partial v}{\partial\theta}\right)-\rho_R A_R\ddot{w}+\rho_R\frac{I^z}{a^2}\frac{\partial^2\ddot{w}}{\partial\theta^2} \tag{33}$$

$$N_z^R(z,\theta) = \frac{G_R C_T}{a^3}\left(\frac{1}{a}\frac{\partial^2 u}{\partial\theta^2}+\frac{\partial^3 w}{\partial z\,\partial\theta^2}\right)+\frac{E_R I_r}{a^3}\left(\frac{\partial^3 w}{\partial z\,\partial\theta^2}-\frac{1}{a}\frac{\partial^4 u}{\partial\theta^4}\right)-\rho_R A_R\ddot{u} \tag{34}$$

$$S_z^R(z,\theta) = \frac{E_R A_R}{a^2}\left(\frac{\partial w}{\partial\theta}+\frac{\partial^2 v}{\partial\theta^2}\right)-\rho_R A_R\ddot{v} \tag{35}$$

For an elastic ring located at the end of the shell, the boundary condition reduces to:

$$\int_{t_1}^{t_2}\int_0^{2\pi}\left[(N_z^R\mp N_z)\delta u+(S_z^R\mp S_z)\delta v+(V_z^R\mp V_z)\delta w-(M_z^R\mp M_z)\delta\left(\frac{\partial w}{\partial z}\right)\right]_{z_R=0}^{z_R=l}a\,\mathrm{d}\theta\,\mathrm{d}t = 0 \tag{36}$$

The top sign on the ring terms corresponds to a stiffener located at $z_R = l$, while the bottom is for $z_R = 0$. The sign reversal occurs to be consistent with the outer normal in Fig. 2. As they appear in the diagram, the boundary loads in eqns (21)–(24) are positive at the end $z = l$. On the opposite side of the shell element, however, all internal forces have the same definitions but each reverse their orientation. Thus, it must be specified at which end the ring appears in order to apply the correct boundary conditions. This is not a concern for a free end, as switching the sign on a quantity set equal to zero does not affect the result.

Once the four internal force balances have been nondimensionalized, Q matrix entries can be derived for the elastic ring stiffener end condition. Analogous to Table 2, the coefficient matrix

Table 3
Coefficient matrix Q entries for the non-axisymmetric modes ($n > 0$) with an elastic ring stiffener on a cylindrical shell ending/beginning (top sign/bottom sign) at $z_R = \Delta a$

Condition for	$Q_{*,r}$ $(r = 1, \ldots, 4)$
$S_z^R(\Delta a) = \pm S_z(\Delta a)$	$\left\{\frac{\rho_R}{\rho}\frac{A_R}{ha}\Omega^2 B_r \mp \frac{1-\nu}{2}[nC_r + (1+\beta^2)\alpha_r B_r - 2\beta^2 n\alpha_r] + (1-\nu^2)\frac{E_R}{E}\frac{A_R}{ha}n(1-nB_r)\right\}e^{\alpha_r\Delta}$
$N_z^R(\Delta a) = \pm N_z(\Delta a)$	$\left\{-(1-\nu^2)\frac{E_R}{E}n^2\left[\frac{I^r}{ha^3}(\alpha_r + n^2 C_r) + \frac{C_T}{2ha^3(1+\nu_R)}(\alpha_r + C_r)\right] + \frac{\rho_R}{\rho}\frac{A_R}{ha}\Omega^2 C_r \mp C_r\alpha_r \mp \nu(1-nB_r)\right\}e^{\alpha_r\Delta}$
$V_z^R(\Delta a) = \pm V_z(\Delta a)$	$\left\{\frac{\rho_R}{\rho}\left(\frac{A_R}{ha} + n^2\frac{I^z}{ha^3}\right)\Omega^2 \pm \beta^2\alpha_r[\alpha_r^2 + nB_r - (2-\nu)n^2] + (1-\nu^2)\frac{E_R}{E}\left[\frac{I^z}{ha^3}(2n^2 - n^4 - 1) + \frac{A_R}{ha}(nB_r - 1)\right]\right\}e^{\alpha_r\Delta}$
$M_z^R(\Delta a) = \pm M_z(\Delta a)$	$\left\{(1-\nu^2)\frac{E_R}{E}\left[\frac{I^r}{ha^3}(\alpha_r + n^2 C_r) + \frac{C_T}{2ha^3(1+\nu_R)}n^2(\alpha_r + C_r)\right] \pm \beta^2[\alpha_r^2 + \nu n(B_r - n)] - \frac{\rho_R}{\rho}\frac{I^\theta}{ha^3}\Omega^2\alpha_r\right\}e^{\alpha_r\Delta}$
Condition for	$Q_{*,r}$ $(r = 5, \ldots, 8)$
$S_z^R(\Delta a) = \pm S_z(\Delta a)$	$\left\{\frac{\rho_R}{\rho}\frac{A_R}{ha}\Omega^2 B_r \pm \frac{1-\nu}{2}[nC_r + (1+\beta^2)\alpha_r B_r - 2\beta^2 n\alpha_r] + (1-\nu^2)\frac{E_R}{E}\frac{A_R}{ha}n(1-nB_r)\right\}e^{-\alpha_r\Delta}$
$N_z^R(\Delta a) = \pm N_z(\Delta a)$	$\left\{(1-\nu^2)\frac{E_R}{E}n^2\left[\frac{I^r}{ha^3}(\alpha_r + n^2 C_r) + \frac{C_T}{2ha^3(1+\nu_R)}(\alpha_r + C_r)\right] - \frac{\rho_R}{\rho}\frac{A_R}{ha}\Omega^2 C_r \mp C_r\alpha_r \mp \nu(1-nB_r)\right\}e^{-\alpha_r\Delta}$
$V_z^R(\Delta a) = \pm V_z(\Delta a)$	$\left\{\frac{\rho_R}{\rho}\left(\frac{A_R}{ha} + n^2\frac{I^z}{ha^3}\right)\Omega^2 \mp \beta^2\alpha_r[\alpha_r^2 + nB_r - (2-\nu)n^2] + (1-\nu^2)\frac{E_R}{E}\left[\frac{I^z}{ha^3}(2n^2 - n^4 - 1) + \frac{A_R}{ha}(nB_r - 1)\right]\right\}e^{-\alpha_r\Delta}$
$M_z^R(\Delta a) = \pm M_z(\Delta a)$	$\left\{-(1-\nu^2)\frac{E_R}{E}\left[\frac{I^r}{ha^3}(\alpha_r + n^2 C_r) + \frac{C_T}{2ha^3(1+\nu_R)}n^2(\alpha_r + C_r)\right] \pm \beta^2[\alpha_r^2 + \nu n(B_r - n)] + \frac{\rho_R}{\rho}\frac{I^\theta}{ha^3}\Omega^2\alpha_r\right\}e^{-\alpha_r\Delta}$

entries for the elastic ring are shown in Table 3. For terms with two signs, the top sign is for the ring located at the end of the shell (e.g. for $\Delta = l/a$), while the second is used at the beginning (e.g. for $\Delta = 0$). Axisymmetric conditions can be found by setting $n = 0$.

A special case for the ring stiffener occurs when the material is assumed to be infinitely stiff relative to the shell material. Thus, the ratio E/E_R for such a rigid ring $\to 0$. The boundary

Table 4
Coefficient matrix Q entries for the axisymmetric modes ($n = 0$) with a rigid ring stiffener on a shell ending/beginning (top sign/bottom sign) at $z = \Delta a$

Condition for	Torsional modes (remaining $Q_{*,r} = 0$) $Q_{*,1}$	$Q_{*,5}$
$S_z^R(\Delta a) = \pm S_z(\Delta a)$	$\frac{\rho_R}{\rho}\frac{A_R}{ha}\gamma\cos\gamma\Delta \pm \sin\gamma\Delta$	$\frac{\rho_R}{\rho}\frac{A_R}{ha}\gamma\sin\gamma\Delta \mp \cos\gamma\Delta$
	where $\gamma = \Omega\sqrt{\frac{2}{(1-\nu)(1+\beta^2)}}$	
Condition for	Axial/longitudinal modes (remaining $Q_{*,r} = 0$) $Q_{*,r}$ $(r = 2,3,4)$	$Q_{*,r}$ $(r = 6,7,8)$
$N_z^R(\Delta a) = \pm N_z(\Delta a)$	$\left(\frac{\alpha_r}{\Omega^2+\alpha_r^2}\right)\left(\pm\alpha_r - \frac{\rho_r}{\rho}\frac{A_R}{ha}\Omega^2\right)e^{\alpha_r\Delta}$	$\left(\frac{\alpha_r}{\Omega^2+\alpha_r^2}\right)\left(\pm\alpha_r + \frac{\rho_r}{\rho}\frac{A_R}{ha}\Omega^2\right)e^{-\alpha_r\Delta}$
$W(\Delta a) = 0$	$e^{\alpha_r\Delta}$	$e^{-\alpha_r\Delta}$
$W'(\Delta a) = 0$	$\alpha_r e^{\alpha_r\Delta}$	$-\alpha_r e^{-\alpha_r\Delta}$

conditions for this scenario become a combination of dynamic loads and geometrical constraints. For the axisymmetric case, letting $E_R \to \infty$ in the bending moment balance between (21) and (32) and the transverse shear force balance between (22) and (33) leads to:

$$W' = 0 \tag{37}$$

$$W = 0 \tag{38}$$

where $()'$ denotes $\mathrm{d}()/\mathrm{d}z$. Based on the remaining terms in the boundary expression (36), we have the remaining two axisymmetric rigid ring conditions from the membrane normal and shear force balances:

$$N_z^R \mp N_z\Big|_{\substack{z_R=l\\z_R=0}} = 0 \tag{39}$$

$$S_z^R \mp S_z\Big|_{\substack{z_R=l\\z_R=0}} = 0 \tag{40}$$

Considering the four boundary conditions that arise for the axisymmetric modes, the effect of a rigid ring on the radial displacement is the same as a clamped end. The Q matrix expressions for the axisymmetric modes subject to a rigid ring end condition are given in Table 4.

Unlike the elastic ring case, the bending modes for the rigid ring must be considered separately from the other modes with $n > 1$. For the membrane normal force $N_z = \pm N_z^R$ and membrane shear force $S_z = \pm S_z^R$ balances, letting $E_R \to \infty$ leads to

$$W' + \frac{U}{a} = 0 \tag{41}$$

$$W - V = 0 \tag{42}$$

Since a rigid ring by definition does not deform, the conditions (41) and (42) can also be obtained by requiring the strain energy of the ring in eqn (26) to be zero. Including the information in (41) and (42) in the boundary expression leads to the two remaining internal force conditions:

$$V_z^R + S_z^R \Big|_{\substack{z_R = l \\ z_R = 0}} = \pm V_z \pm S_z \Big|_{\substack{z_R = l \\ z_R = 0}} \tag{43}$$

$$M_z^R + aN_z^R \Big|_{\substack{z_R = l \\ z_R = 0}} = \pm M_z \pm aN_z \Big|_{\substack{z_R = l \\ z_R = 0}} \tag{44}$$

For the vibration modes with $n > 1$, it can be easily shown that the only displacements that satisfy the force balances are the same as those for a clamped end, whose associated matrix entries are given in Table 2. Thus, the only difference between a rigid ring stiffener and a clamped end is their effect on the axisymmetric and bending modes. This observation is also made by Ludwig and Krieg (1981) and served as an upper limit check for an elastic ring with a large yet finite Young's modulus. The relevant Q matrix entries for the bending modes with a rigid ring end condition are shown in Table 5.

Table 5
Coefficient matrix Q entries for the bending modes ($n = 1$) with a rigid ring stiffener on a shell ending/beginning (top sign/bottom sign) at $z = \Delta a$

Condition for	$Q_{*,r}$ $(r = 1, \ldots, 4)$
$V(\Delta a) - W(\Delta a) = 0$	$(1 - B_r)\, e^{\alpha_r \Delta}$
$U(\Delta a) + aW'(\Delta a) = 0$	$(C_r + \alpha_r)\, e^{\alpha_r \Delta}$
$V_z^R(\Delta a) + S_z^R(\Delta a) = \pm V_z(\Delta a) \pm S_z(\Delta a)$	$\left\{ \frac{\rho_R}{\rho} \Omega^2 \left[2\frac{A_R}{ha} + \frac{I^z}{ha^3} \right] \pm \beta^2 \alpha_r [\alpha_r^2 + B_r - (2 - \nu)] \mp \frac{1 - \nu}{2} [C_r + B_r \alpha_r (1 + \beta^2) - 2\beta^2 \alpha_r] \right\} e^{\alpha_r \Delta}$
$M_z^R(\Delta a) + aN_z^R(\Delta a) = \pm M_z(\Delta a) \pm aN_z(\Delta a)$	$\left\{ \pm \alpha_r (\alpha_r \beta^2 - C_r) - \frac{\rho_R}{\rho} \Omega^2 \left[\frac{A_R}{ha} + \frac{I^\theta}{ha^3} \right] \alpha_r \right\} e^{\alpha_r \Delta}$
Condition for	$Q_{*,r}$ $(r = 5, \ldots, 8)$
$V(\Delta a) - W(\Delta a) = 0$	$(1 - B_r)\, e^{-\alpha_r \Delta}$
$U(\Delta a) + aW'(\Delta a) = 0$	$-(C_r + \alpha_r)\, e^{-\alpha_r \Delta}$
$V_z^R(\Delta a) + S_z^R(\Delta a) = \pm V_z(\Delta a) \pm S_z(\Delta a)$	$\left\{ \frac{\rho_R}{\rho} \Omega^2 \left[2\frac{A_R}{ha} + \frac{I^z}{ha^3} \right] \mp \beta^2 \alpha_r [\alpha_r^2 + B_r - (2 - \nu)] \pm \frac{1 - \nu}{2} [C_r + B_r \alpha_r (1 + \beta^2) - 2\beta^2 \alpha_r] \right\} e^{-\alpha_r \Delta}$
$M_z^R(\Delta a) + aN_z^R(\Delta a) = \pm M_z(\Delta a) \pm aN_z(\Delta a)$	$\left\{ \pm \alpha_r (\alpha_r \beta^2 - C_r) + \frac{\rho_R}{\rho} \Omega^2 \left[\frac{A_R}{ha} + \frac{I^\theta}{ha^3} \right] \alpha_r \right\} e^{-\alpha_r \Delta}$

Other boundary conditions are certainly possible, such as springs or end masses. These can be easily dealt with as long as they can be expressed in terms of the shell displacements, from which the entries for Q will follow.

5. Modal orthogonality and normalization

When the boundary conditions are such that the natural modes are orthogonal, then modal analysis reduces the three partial differential equations of motion to a single harmonic oscillator equation for each mode. We will use the approach taken by Meirovitch (1967) for beams and plates, in which the stiffness operator is integrated by parts. If the boundary terms vanish, then the mode shapes are orthogonal. For two mode shapes $\{\mathscr{U}_i\}$ and $\{\mathscr{U}_k\}$ with respective circumferential mode numbers p and n, the orthogonality condition follows from

$$\int_{\mathscr{A}} \{\mathscr{U}_k\}^T L[\mathscr{U}_i]\,\mathrm{d}\mathscr{A} - \int_{\mathscr{A}} \{\mathscr{U}_i\}^T L[\mathscr{U}_k]\,\mathrm{d}\mathscr{A} = (\omega_i^2 - \omega_k^2) \int_{\mathscr{A}} \{\mathscr{U}_k\}^T \mathscr{M} \{\mathscr{U}_i\}\,\mathrm{d}\mathscr{A} \tag{45}$$

where $\mathscr{A}$ is the domain of the shell mid-plane and $\mathrm{d}\mathscr{A} = a\,\mathrm{d}\theta\,\mathrm{d}z$. Whenever the left hand side vanishes and $\omega_i \neq \omega_k$, then the mode shapes $\{\mathscr{U}_k\}$ and $\{\mathscr{U}_i\}$ are orthogonal. This is equivalent to requiring that the stiffness operator be self-adjoint within the domain defined by the shell mid-plane. Furthermore, a self-adjoint operator is guaranteed to have real eigenvalues (see e.g. Greenberg, 1978), yielding real-valued natural frequencies. After integration by parts, one obtains the following expression:

$$\begin{aligned}
&\int_{\mathscr{A}} \{\mathscr{U}_k\}^T L[\mathscr{U}_i]\,\mathrm{d}\mathscr{A} - \int_{\mathscr{A}} \{\mathscr{U}_i\}^T L[\mathscr{U}_k]\,\mathrm{d}\mathscr{A} \\
&\quad = -\frac{Eha}{1-\nu^2} \left\{ \int_0^{2\pi} \sin n\theta \sin p\theta\,\mathrm{d}\theta \left[U_k U_i' - U_k' U_i - \frac{1+\nu}{2a} n U_k V_i + \frac{\nu}{a} U_k W_i \right]_0^l \right. \\
&\quad + \int_0^{2\pi} \cos n\theta \cos p\theta\,\mathrm{d}\theta \left[\frac{1+\nu}{2a} n V_k U_i + (1+\beta^2) \frac{1-\nu}{2} (V_k V_i' - V_k' V_i) \right. \\
&\quad \left. - \beta^2 n (V_k W_i' - V_k' W_i) \right]_0^l + \int_0^{2\pi} \sin n\theta \sin p\theta\,\mathrm{d}\theta \left[-\frac{\nu}{a} W_k U_i - \beta^2 n (W_k V_i' - W_k' V_i) \right. \\
&\quad \left. \left. + 2n^2\beta^2 (W_k W_i' - W_k' W_i) - \beta^2 a^2 (W_k W_i''' - W_k' W_i'' + W_k'' W_i' - W_k''' W_i) \right]_0^l \right\}
\end{aligned} \tag{46}$$

For two modes with different circumferential mode number, the right hand side of (46) vanishes due to the periodicity and orthogonality of the sine and cosine functions. For two modes with the same circumferential mode number, the orthogonality condition can be simplified to the following:

$$\int_{\mathscr{A}} \{\mathscr{U}_k\}^T L[\mathscr{U}_i]\,\mathrm{d}\mathscr{A} - \int_{\mathscr{A}} \{\mathscr{U}_i\}^T L[\mathscr{U}_k]\,\mathrm{d}\mathscr{A}$$

$$= -ca[U_k N_z^i - U_i N_z^k + V_k S_z^i - V_i S_z^k + W_k V_z^i - W_i V_z^k - W'_k M_z^i + W'_i M_z^k]_0^l \quad (47)$$

where the boundary terms are recognized as the products of the geometric boundary conditions and their associated internal forces. The constant c is 2π when considering two axisymmetric modes and π otherwise. Any combination of edge conditions that causes this collection of boundary terms to vanish yields orthogonal modes. Equation (47) shows that the orthogonality of the natural modes can be reduced to the vanishing of a collection of boundary terms. These products all have the form of a displacement or slope multiplied by its associated internal force or moment. This reduction is intuitive, since it can be done for most distributed parameter systems (beams, plates, etc.). If a displacement is specified to be some value on the boundary, then its corresponding internal force must remain unknown until the problem has been solved, and vice versa.

In the case of an elastic ring stiffener, it can be shown that substituting the internal force expressions (32)–(35) into eqn (47) causes the right-hand side to vanish identically. In fact, switching the sign on each ring load also leads to orthogonal modes. As mentioned in the previous section, this is important because the signs on the effective ring forces may change direction, depending on which end of the shell to which the ring is attached. Since the rigid ring stiffener is a limiting case for this scenario, it also leads to orthogonal modes when present. It should be noted that the effective internal forces derived here will lead to orthogonal modes for any shell theory that satisfies (47). This is so because the ring loads were derived here regardless of the form of the internal forces provided by the shell theory. Only the equating of these expressions was done here. If the boundary expression is satisfied for the classical fixed/free end combinations, then it will also work with the effective ring forces derived here. Thus, the elastic ring end conditions derived here will also work with the shell theories of Morley-Koiter, Sanders, and Flügge, to name a few, because each of these will satisfy the boundary expression (47). This can also be verified using MAPLE to keep track of the numerous terms that develop.

Linear springs can also be accommodated through the boundary conditions. Assuming that they are fixed to some ground reference, restoring forces imposed by linear springs are simply the displacements themselves multiplied by the associated spring constants. It is easy to verify that this causes the right-hand side of (47) to disappear, rendering the modes orthogonal.

For completeness, orthogonality must be established between the rigid body modes and all of the other types. There are several combinations to consider. Before we proceed, however, it is easy to verify that for the first three rigid body modes in Table 1, the internal forces defined by eqns (21)–(24) vanish throughout the shell. For the transverse rotational mode, however, the membrane normal and bending moment vanish throughout, but the membrane and transverse shear forces are independent non-zero values, given by

$$V_z(z,\theta) = -\sqrt{12}\frac{E\beta^3}{1+\nu}\mathscr{C}\begin{cases}\sin\theta\\ \cos\theta\end{cases} \quad S_z(z,\theta) = \frac{\sqrt{12}}{2}\frac{E\beta^3}{1+\nu}\mathscr{C}\begin{cases}\cos\theta\\ -\sin\theta\end{cases}$$

where $\mathscr{C}$ is the arbitrary constant used in Table 1. Another result that we will need for the bending modes is the relation between the radial and circumferential displacements whenever both the bending moment and transverse shear force vanish simultaneously. When this occurs for the

bending modes, integrating (22) with respect to z and then subtracting (21) leads to the following relation:

$$V(z)-2W(z)=\text{constant}, \quad \text{for } n=1 \text{ and both } M_z(z,\theta)=0 \text{ and } V_z(z,\theta)=0 \tag{48}$$

The two axisymmetric rigid body modes are orthogonal to all modes with $n>0$ due to the periodicity of the sine and cosine functions, regardless of the boundary conditions. When compared to other axisymmetric modes, however, we must consider what boundary conditions will cause the rigid body modes to be present. In this case, let the index k correspond to the axisymmetric rigid body mode and i correspond to any other axisymmetric mode. For zero membrane normal at each end of the shell, the rigid body mode for pure axial translation is present. Since the membrane normal for this rigid body mode is zero throughout the body, including the ends, the boundary terms in (47) corresponding to the longitudinal displacement disappear. For zero membrane shear at each end, the rigid body mode for pure axial rotation is present. Since the membrane shear for this mode is zero throughout the body, including the ends, the boundary terms in (47) corresponding to the circumferential displacement vanish. Therefore, the two axisymmetric rigid body modes will be orthogonal to all other modes when the boundary conditions are such that they exist.

Both the transverse translation and rotation mode are orthogonal to all modes with $n\neq 1$ due to the orthogonality and periodicity of the sine and cosine functions, regardless of the end conditions. When compared to other bending modes, however, we must consider what boundary conditions will cause these rigid body modes to be present. In this case, let the index k correspond to the rigid body bending mode and i correspond to any other bending mode. For free–free end conditions, the rigid body bending modes will also be present. Since the internal forces for the transverse translation rigid body mode are zero throughout the shell, all terms in (47) vanish, proving orthogonality. Between the transverse rotation mode and other bending modes, however, the boundary terms do not all vanish as simply. Due to the observation in (48), eqn (47) reduces to

$$\int_{\mathscr{D}} \{\mathscr{U}_k\}^T L[\mathscr{U}_i]\,\mathrm{d}\mathscr{D} - \int_{\mathscr{D}} \{\mathscr{U}_i\}^T L[\mathscr{U}_k]\,\mathrm{d}\mathscr{D} = \pi a[V_i S_z^k + W_i V_z^k]_0^l = \pi a[S_z^k(V_i-2W_i)]_0^l \tag{49}$$

Recalling that the membrane shear force is the same at both ends of the shell and using the result obtained in (48), the remaining boundary terms vanish, completing the final proof for modal orthogonality. Thus, the two rigid body bending modes will be orthogonal to all other modes when the boundary conditions are such that they exist.

Now that all the natural modes have been shown to be orthogonal for the several cases considered, the next step is to normalize them. Since the mode shapes can be determined to within a multiplicative constant, the arbitrariness is avoided by normalizing the modes according to

$$\int_{\mathscr{D}} \{\mathscr{U}_k\}^T \mathscr{M}\{\mathscr{U}_k\}\,\mathrm{d}\mathscr{D} = 1 \tag{50}$$

Combining (50) with the modal orthogonality gives the following relations for modes with different frequencies:

$$\int_{\mathscr{D}} \{\mathscr{U}_i\}^T \mathscr{M} \{\mathscr{U}_k\} \, \mathrm{d}\mathscr{D} = \delta_{ik} \tag{51}$$

$$\int_{\mathscr{D}} \{\mathscr{U}_i\}^T L[\mathscr{U}_k] \, \mathrm{d}\mathscr{D} = \omega_k^2 \delta_{ik} \tag{52}$$

where δ_{ik} is the Kronecker delta. Substituting the modal expansion (5) into the equations of motion, premultiplying by $\mathscr{U}_k^T$, integrating over the shell surface and employing (51) and (52) lead to the modal coordinate equations:

$$\ddot{\eta}_k(t) + \omega_k^2 \eta_k(t) = \int_0^l \int_0^{2\pi} \mathscr{U}_k^T(z,\theta) \mathscr{F}(z,\theta,t) a \, \mathrm{d}\theta \, \mathrm{d}z \tag{53}$$

The orthonormality of the modes reduces the three partial differential equations to uncoupled harmonic oscillators for each of the natural modes.

As shown earlier, all non-zero circumferential mode numbers have a degeneracy of two, due to the circular symmetry of the cross-section. For two modes with equal natural frequencies, choosing them to have the forms of (7) and (8) will produce the desired result due to the orthogonality of sine and cosine functions. Applying the orthonormality relations (51) and (52) leads to the following general modal displacements for each mode with $n > 0$:

$$u(z,\theta) = \frac{1}{\sqrt{\pi \rho h a^2}} \sum_{r=1}^{4} C_r \{A_r \, \mathrm{e}^{\alpha_r z/a} - A_r' \, \mathrm{e}^{-\alpha_r z/a}\} \begin{cases} \sin n\theta \\ \cos n\theta \end{cases}$$

$$v(z,\theta) = \frac{1}{\sqrt{\pi \rho h a^2}} \sum_{r=1}^{4} B_r \{A_r \, \mathrm{e}^{\alpha_r z/a} + A_r' \, \mathrm{e}^{-\alpha_r z/a}\} \begin{cases} \cos n\theta \\ -\sin n\theta \end{cases}$$

$$w(z,\theta) = \frac{1}{\sqrt{\pi \rho h a^2}} \sum_{r=1}^{4} \{A_r \, \mathrm{e}^{\alpha_r z/a} + A_r' \, \mathrm{e}^{-\alpha_r z/a}\} \begin{cases} \sin n\theta \\ \cos n\theta \end{cases}$$

For the axisymmetric modes, the normalization constants for the torsional modes can be found independently and depend on the boundary conditions.

$$u(z,\theta) = w(z,\theta) = 0, \quad v(z,\theta) = \frac{1}{\sqrt{2\pi \rho h a^2}} \left[A_1 \cos\left(\gamma \frac{z}{a}\right) + A_1' \sin\left(\gamma \frac{z}{a}\right) \right] \tag{54}$$

For the radial/longitudinal modes, the general normalized form can be simplified to

$$u(z,\theta) = \frac{1}{\sqrt{2\pi \rho h a^2}} \sum_{r=2}^{4} \frac{\nu \alpha_r}{\Omega^2 + \alpha_r^2} \{A_r' \, \mathrm{e}^{-\alpha_r z/a} - A_r \, \mathrm{e}^{\alpha_r z/a}\}$$

$$v(z,\theta) = 0$$

$$w(z,\theta) = \frac{1}{\sqrt{2\pi \rho h a^2}} \sum_{r=2}^{4} \{A_r \, \mathrm{e}^{\alpha_r z/a} + A_r' \, \mathrm{e}^{-\alpha_r z/a}\}$$

The rigid body modes can also be normalized according to eqn (51).

6. Application of commercial software

Two popular commercial software packages were used to facilitate the cylindrical shell eigensolution. MAPLE was used for its symbolic manipulation capability. Soedel's formulation (1981) was coded into a MAPLE file in its original form, regardless of the shell geometry. Once this is done, substituting the appropriate Lamé parameters and radii of curvature lead to the equations of motion for the desired geometry. For a circular cylindrical shell, the equations of motion that result are also those obtained by Junger and Feit (1972). Using this procedure, the natural boundary forces associated with the shell deflections can also be determined. As mentioned earlier, deriving the boundary conditions consistent with the equations of motion is necessary to ensure the modal orthogonality of the eigensolution. With the governing equations defined within MAPLE, the general form of the displacements was substituted into the equations of motion to obtain relation (10). A common practice at this point is to assume the nature of the axial mode number m before continuing, such as $\alpha = m\pi a\sqrt{-1}/l$ for the freely supported case. Once this has been done, the determinant of the coefficient matrix in eqn (10) leads to three roots for Ω for the given axial mode number. Associated with each of these values are cases in which each of the primary shell motions dominates. The assumption of the axial mode number dependence is usually done because the roots of the determinant cannot be done in closed form. Using MAPLE, however, the roots of the characteristic equation can be carried throughout the procedure. The values of the shell parameters can be substituted in at a later time, without prior knowledge of α. The determinant of the coefficient matrix set to zero becomes the characteristic equation for α. For a specified set of v, h/a, and l/a, the only remaining unknown is the frequency parameter Ω. Knowing that the values of α that satisfy this equation render the coefficient matrix singular, MAPLE was also used to generate expressions for B and C by solving the first two of the three equations contained in (10).

The second task of MAPLE was to handle the wide variety of boundary conditions considered in this study. To do this, MAPLE routines were written to take any desired combination of boundary conditions and generate the associated coefficient matrix entries given in Tables 2–5. A summary of scenarios encountered with the boundary conditions examined here are shown in Table 6. MAPLE was also used to verify the collection of boundary terms on the right hand side of eqn (47) for the shell theories of Junger and Feit, Morley-Koiter, Sanders, and Flügge.

MATLAB was used for its ability to do large scale matrix manipulations and number crunching. All expressions generated by MAPLE were written to files in MATLAB script format. Regardless of the complexity of the MAPLE expressions, MATLAB can quickly evaluate their values, provided that all variables included within the expression are currently defined. Once boundary conditions and the ratios for v, h/a, and l/a are prescribed, the eigenvalue problem can be solved. The difficulty in solving the eigenvalue problem is that the boundary coefficient matrix Q can become ill-conditioned due to the exponential terms. Furthermore, the characteristic equation that results involves computing the determinant of this 8×8 matrix, a task beyond even MAPLE's capability for the general case. Once the eight boundary conditions are specified, the solution results by simultaneously obtaining the zeroes of both the characteristic equations for the 3×3 displacement coefficient matrix and the 8×8 boundary determinant. Since this is not feasible in closed form, we chose to iterate through a range for Ω, at each step solving the 3×3 displacement determinant for α and substituting it into the boundary coefficient matrix. After a desired frequency

Table 6
Boundary value subproblems that arise for the end conditions investigated

Scenario	Axisymmetric modes ($n = 0$)		Non-axisymmetric modes ($n > 0$)	
Fixed/free boundary conditions	Torsion decouples, 2 conditions on $V(z)$, 2×2 subproblem	Axial/long. modes, 6 end conditions, 6×6 subproblem	Full eigenvalue problem, 8 boundary conditions, 8×8 coefficient matrix	
Elastic ring stiffener	Torsion decouples, 2 conditions on $V(z)$, 2×2 subproblem	Axial/long. modes, 6 end conditions, 6×6 subproblem	Full eigenvalue problem, 8 boundary conditions, 8×8 coefficient matrix	
Rigid ring stiffener	Torsion decouples, 2 conditions on $V(z)$, 2×2 subproblem	Axial/long. modes, 6 end conditions, 6×6 subproblem	Bending ($n = 1$)	Higher ($n > 1$)
			8 conditions, 8×8 matrix	8 conditions, treat as clamped end

band for Ω is chosen, another MATLAB script file was written to sweep through this range, solving for the roots of α and the values of B and C at each step. The determinant of the boundary coefficient matrix will be a complex number using this approach, so the behavior of the modulus of the determinant is monitored by MATLAB at each step in the frequency band. Numerically, the frequencies show up as inverted spikes when the magnitude of the determinant is plotted vs frequency. Therefore, the MATLAB code simply has to check for these spikes and record when they occur.

Once the frequencies have been located within a given range, the mode shapes must be determined next. At each of the frequencies obtained by the first MATLAB code, the values of α, B, and C are recalled. Since the determinant of the coefficient matrix is singular at these locations, the value of A_4' is set to unity and MATLAB solves for the remaining seven constants using the first seven equations contained in (25). Once this is done, the modal coefficients are then normalized according to eqn (50). This is done by numerically integrating the left hand side of (50) using MATLAB. All values of A_i and A_i' are subsequently multiplied by the inverse square root of the value of this integral. This step normalizes the displacements with respect to the inner product, but they may still be complex valued. In order to obtain real-valued displacements, they are also multiplied by a complex rotation mapping $e^{\phi\sqrt{-1}}$, where ϕ is an angle determined to bring the displacements back to the real line. Both the modal displacements and their associated internal forces can be viewed within MATLAB.

7. Experimental validation

Before we use the procedure developed here for parametric shell studies, we will confirm that solving the equations of motion developed by Junger and Feit will produce frequencies observed in experiment. Using their theory, Callahan (1997) showed excellent agreement between the present solution methodology and all of the experimental work cited in the Introduction. Although

Table 7
Eigenvalues for a beam with various boundary conditions

Boundary conditions	λ_m 1	2	3	4	5	>5
Clamped–clamped	4.730	7.853	11.00	14.14	17.28	$(2m+1)\pi/2$
Clamped–free	1.875	4.694	7.855	11.00	14.14	$(2m-1)\pi/2$
Hinged–hinged	3.142	6.283	9.425	12.57	15.71	$m\pi$
Free–free	0	0	4.730	7.853	11.00	$(2m-3)\pi/2$

significantly more experimental papers exist in the literature, comparison is only possible with those studies that gave actual tabulated values of observed resonant frequencies. Here, we shall limit discussion to only three of these cases.

For cylindrical shell modes in which the radial deflection dominates, Soedel (1980) derived an expression for the natural frequencies which depends on the ratios v, h/a, and l/a, the circumferential mode number n, and the axial mode eigenvalues of the analogous beam vibration problem. In order to compare Soedel's expression with the nondimensionalized frequency Ω, it can be rearranged into the following form:

$$\Omega^2 = \beta^2 \left[n^2 + \lambda_m^2 \left(\frac{a}{l}\right)^2 \right]^2 + (1-v^2) \frac{\lambda_m^4}{\left[n^2 \left(\frac{l}{a}\right)^2 + \lambda_m^2 \right]^2} \tag{55}$$

where the values of λ_m ($m = 1, 2, \ldots$) are the eigenvalues of the associated beam vibration problem. When appropriate, this expression will be shown in addition to the experimental data and the values obtained using the procedure outlined in this paper. For reference, the eigenvalues for various sets of boundary conditions treated by Inman (1994) are shown in Table 7.

The first comparison will be with the clamped–clamped experiment done by Koval and Cranch (1962). They used material properties for mild steel, with $E = 206$ GPa, $\rho = 7850$ kg/m^3, and $v = 0.3$. The shell dimensions from their experiment were $a = 76.2$ mm, $h = 0.254$ mm, and $l = 304.8$ mm. They obtained experimental frequencies for the first five axial modes with circumferential mode number in the range $3 \leqslant n \leqslant 14$. Figure 3 shows the comparison between Soedel's approximation, the experimental data, and the results obtained in this paper. The agreement between Soedel's eqn (55) and experiment is very good because the shell is very thin compared to its radius. This causes the radial modes to dominate in the experimentally tested bandwidths.

The second thin shell case we will consider is the clamped–free shell experiment done by Khadakkar et al. (1988). The material used in this shell was mild steel, with the typical material properties $E = 207$ GPa, $\rho = 7860$ kg/m^3, and $v = 0.28$. The shell dimensions from their experiment are $a = 32.25$ mm, $h = 1.5$ mm, and $l = 254$ mm. They obtained experimental frequencies for the first five axial modes with $1 \leqslant n \leqslant 4$. Figure 4 shows the comparison between Soedel's approximation, the experimental data, and the results obtained in the present study. As discussed by

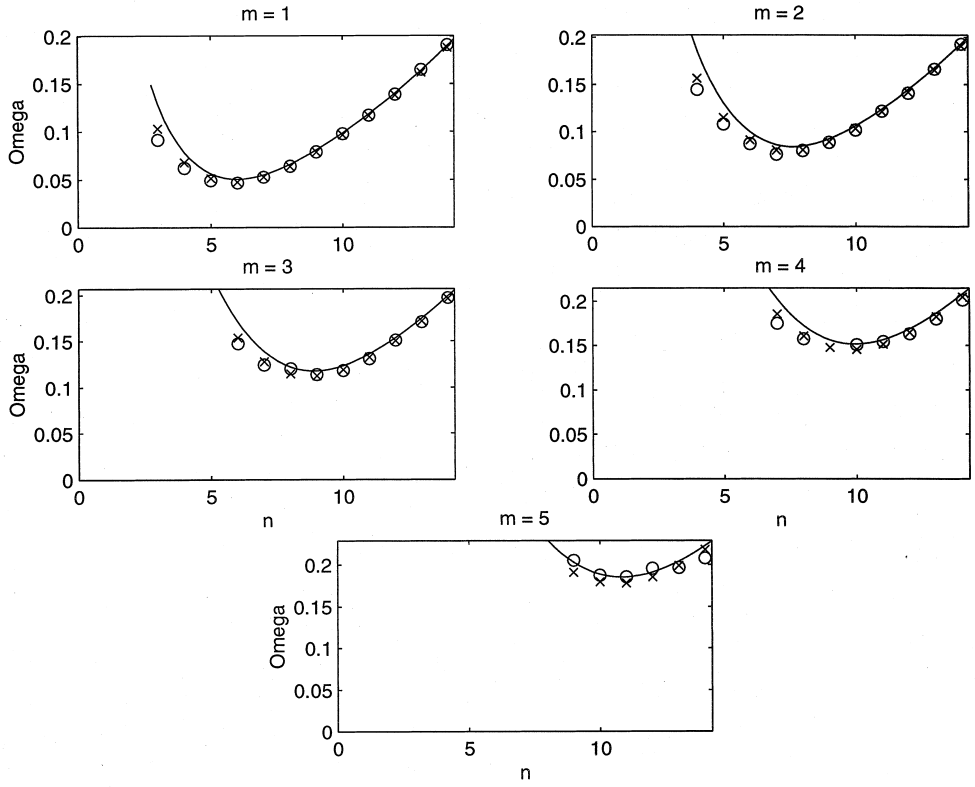

Fig. 3. Nondimensional frequency Ω vs mode numbers m and n according to Koval and Cranch (○), Soedel's equation (—), and the present approach (×).

Soedel in his paper, the accuracy of eqn (55) increases with growing n for a given axial mode number.

The final experimental comparison uses the elastic ring–elastic ring shell results obtained by El Raheb and Babcock (1981). They used aluminum with the properties $E = 68.2$ GPa, $\rho = 2700$ kg/m^3, $v = 0.33$, and integral rings machined into the shell to achieve the elastic ring end conditions. The shell dimensions from their experiment are $a = 102.0$ mm, $h = 0.365 \pm 0.022$ mm, and $l = 177.8$ mm. They created a ring with rectangular cross-section, with the dimensions shown in Fig. 5. Using these values, the ring parameters become:

$$e = 0.0330, \quad b = 0.0747$$

$$\frac{A_R}{ha} = 2.9098, \quad \frac{I_G^z}{ha^3} = 0.0012 \quad \frac{I_G^\theta}{ha^3} = 0.0066, \quad \frac{I_G^r}{ha^3} = 0.0054 \quad \frac{C_T}{ha^3} = 0.0035, \quad \frac{E_R}{E} = \frac{\rho_R}{\rho} = 1$$

Figure 6 shows the experimental data plotted with the frequency predictions generated by the present approach. Also shown are the frequency predictions corresponding to true clamped conditions. At lower values of n, the clamped end produces frequencies significantly higher than the elastic ring case, but becomes an adequate approximation as it increases. The authors estimated

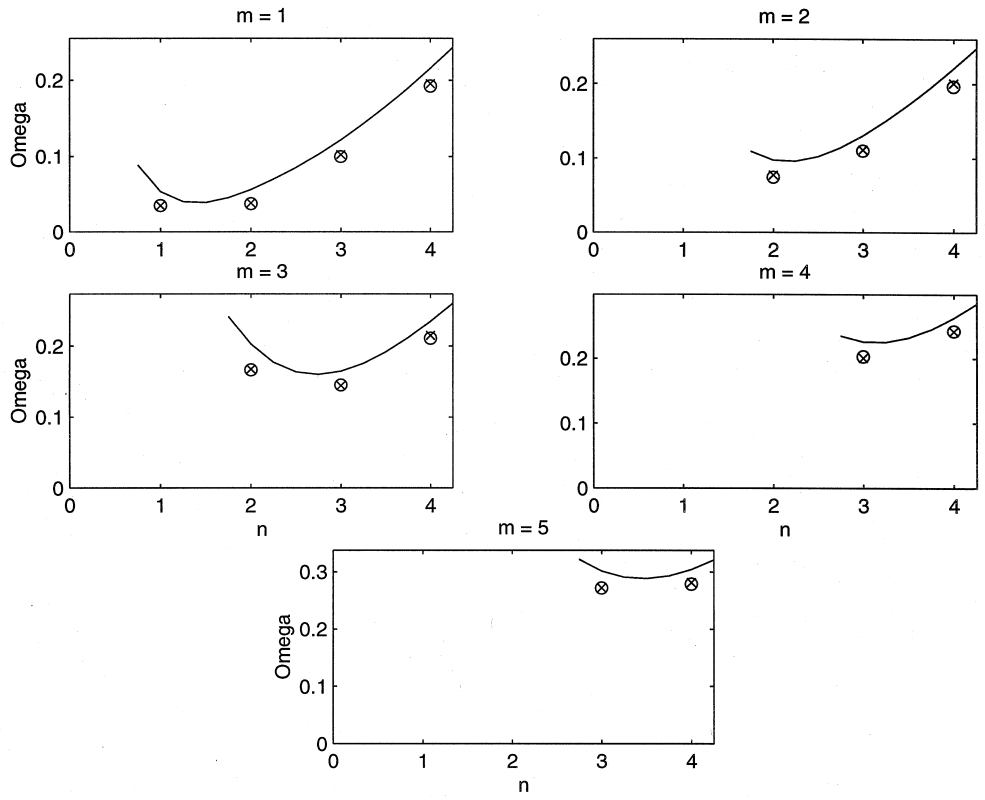

Fig. 4. Nondimensional frequency Ω vs mode numbers m and n according to Khadakkar et al. (○), Soedel's equation (—), and the present approach (×).

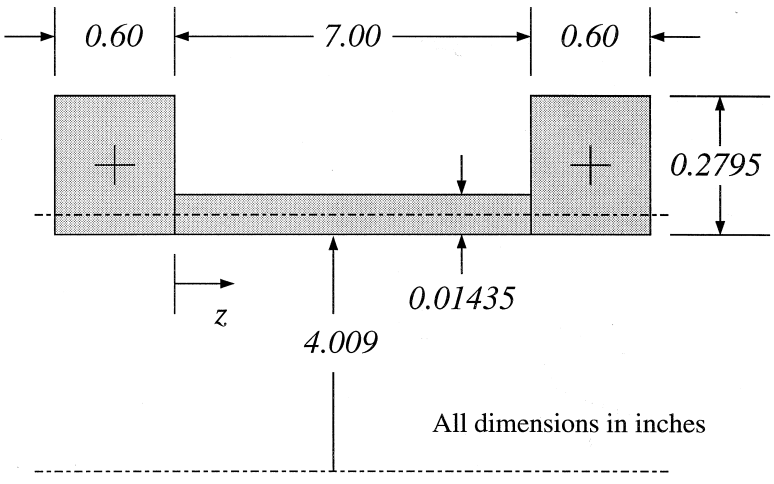

Fig. 5. Schematic diagram of the cylindrical shell used by El Raheb and Babcock.

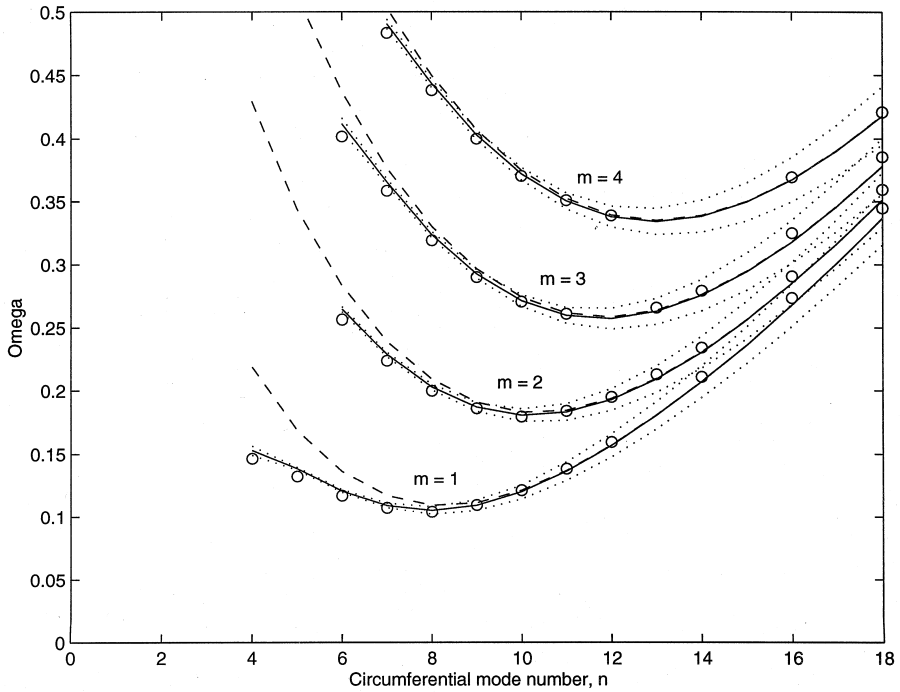

Fig. 6. Nondimensional frequency Ω vs mode numbers m and n according to El Raheb and Babcock (○) and the present approach using elastic ring (—) and clamped (- - -) end conditions.

uncertainty in the shell thickness to be around $\pm 6\%$. These values were also put into the solution procedure, with the results shown in Fig. 6 as the dotted lines. Here, the upper and lower curves are associated with the upper and lower bounds on h. Many of the data points fall within the bounds resulting from the uncertainty in the shell thickness. Figure 6 illustrates the heightened sensitivity of the frequency behavior to small variations in the shell thickness with increasing n. All computed values agree with the experimental data to within $4\frac{1}{2}\%$, well within the uncertainty reported for h.

8. Parametric studies

Now that confidence has been established in the frequency predictions, we can use the present approach to investigate the associated mode shapes. To see the effects of different boundary conditions on the natural mode shapes, we will show some examples. The first case is a clamped–free cylindrical shell with $\nu = 1/3$, $h/a = 1/20$, and $l/a = 3$. Figures 7 and 8 show the first two bending ($n = 1$) and $n = 3$ modes, respectively, for these ratios and the clamped–free boundary conditions. The second example is a free–free cylindrical shell with the same dimensions and Poisson ratio as the previous case. Note immediately that all six rigid body modes given in Table 1 will be present, so the first natural frequency is zero with a degeneracy of six. Some of the first few modes with nonzero natural frequencies are illustrated in Figs 9 and 10.

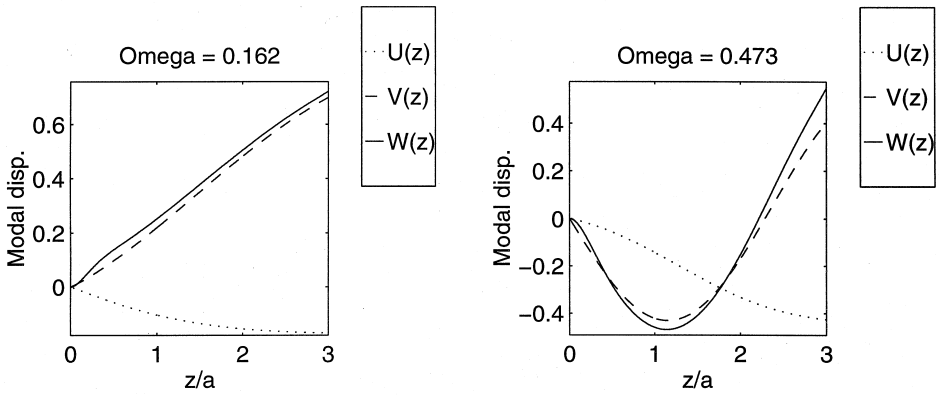

Fig. 7. First two bending modes for a clamped–free shell with $l/a = 3$, $h/a = 1/20$, and $v = 1/3$.

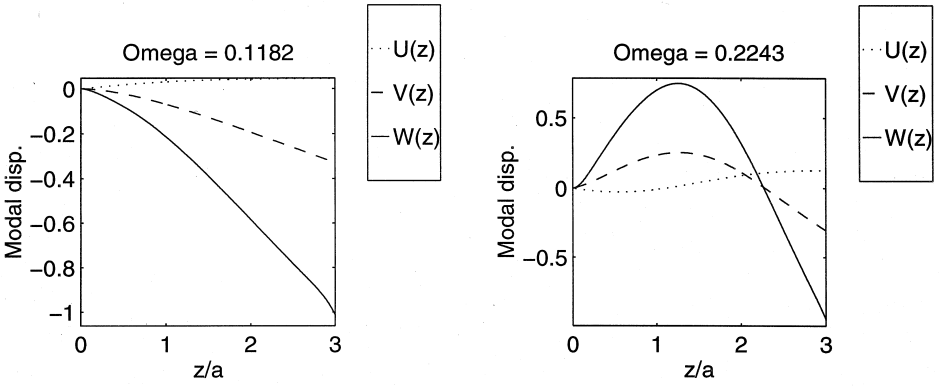

Fig. 8. First two modes with $n = 3$ for a clamped–free shell with $l/a = 3$, $h/a = 1/20$, and $v = 1/3$.

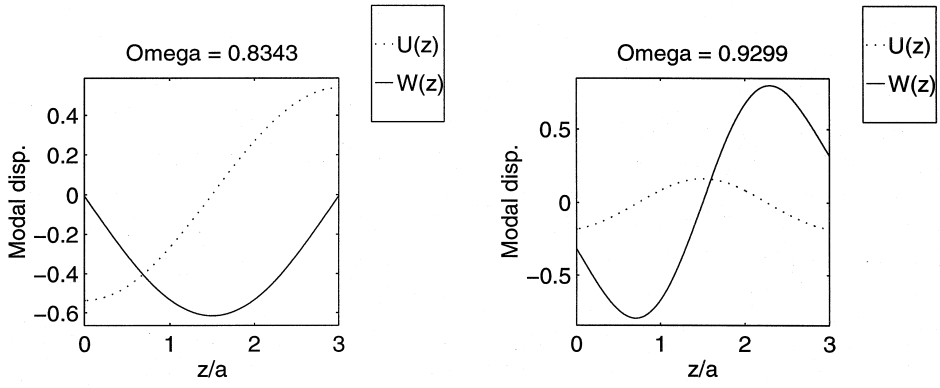

Fig. 9. Fourth and fifth axisymmetric modes (first two are rigid body modes, third is pure torsion) for a free–free shell with $l/a = 3$, $h/a = 1/20$, and $v = 1/3$.

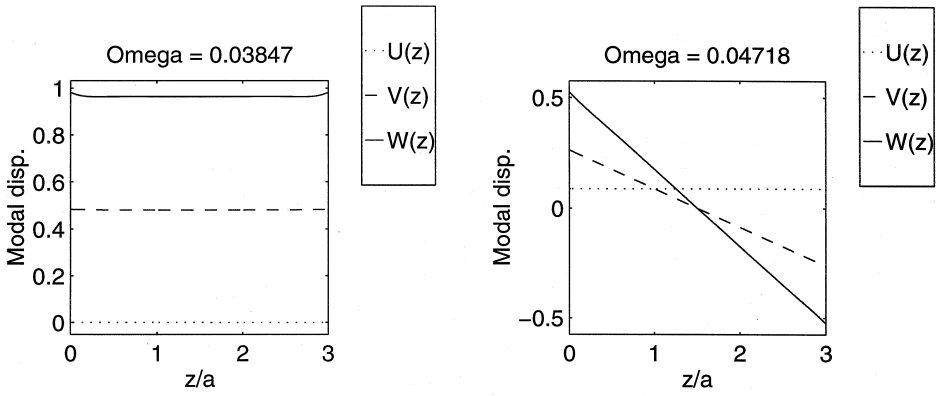

Fig. 10. First two ovalling modes for a free–free shell with $l/a = 3$, $h/a = 1/20$, and $v = 1/3$.

With the present approach coded in MATLAB, it can also be used as a tool to investigate the dependence of the shell frequencies on the mode numbers m and n. For a prescribed set of boundary conditions, the approach developed in this paper can also be used to generate frequency maps, showing the variation in natural frequencies for a particular family of mode types. The benchmark result investigated over the years is the freely-supported shell, whose boundary conditions are:

$$N_z = 0, \quad M_z = 0, \quad \text{and} \quad v = w = 0 \quad \text{at } z = 0, l$$

This is the cylindrical shell analog to the simply-supported beam. For a fixed set of mode numbers m and n, there are three types of motion that can occur. This can be explained by examining the matrix on the left-hand side of eqn (10), whose characteristic equation produces three values of Ω for a fixed α and n. As observed by Soedel (1981), the lowest value is associated with flexurally dominant motion, characterized by radially dominant modeshapes. The other two are usually associated with motion in which stretching or shearing of the tangent plane dominates. Distinguishing between the flexurally dominant and other types can be done by simply observing the nature of the mode shapes. Separation between predominantly axial and torsional modes, however, is more difficult because their deflections are often of comparable magnitudes, especially at lower values of n. Rather than classify the remaining types in this manner, another way is separation into dilatationally and shear dominant modes. This is achieved by examining the volume change, $\varepsilon_{zz} + \varepsilon_{\theta\theta}$, and the in-plane shear, $\varepsilon_{z\theta}$, respectively, at each frequency. The frequencies corresponding to dilatation are usually larger than the shear type given the same mode number m. Thus, for a given mode number pair (m, n), one can find three modal configurations, where flexure, shear, and dilatation of the mid-plane dominates the mode shape, usually in increasing frequency order.

Figure 11 shows the frequency map for a freely-supported shell with $l/a = 3$, $h/a = 1/20$, and $v = 1/3$. Shown in the figure are the first seven flexural and shear modes, as well as the first four dilatational modes. The three types of shell vibration separate into distinct bands of curves as n increases. At lower values of n, the flexural modes are still reasonably distinct, but curves for the other two types overlap in this region, making separation between them difficult. At larger n, axial dominant motion becomes characteristic of the shear dominated modes, while torsional dominance becomes indicative of the dilatational modes. Thus, separating the vibrational modes in either

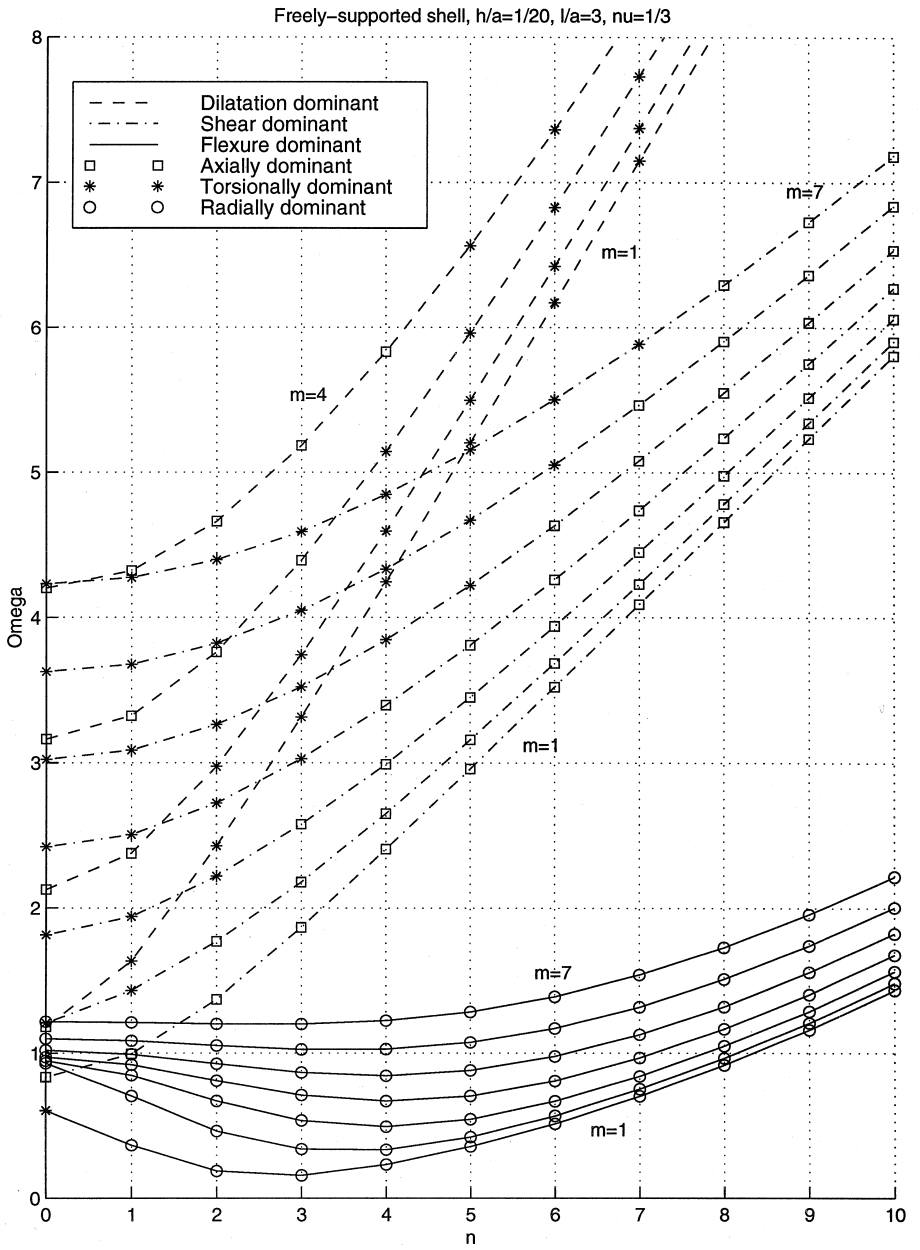

Fig. 11. Nondimensional frequency Ω vs mode numbers m and n for a freely-supported shell with $l/a = 3$, $h/a = 1/20$, and $\nu = 1/3$.

manner produces the same result in this region. At lower n, however, axially or torsionally dominant deformation does not seem to be the best indicator of mode type, as connecting them in this fashion would lead to bizarre frequency trends. It is in this regime that classification into shear

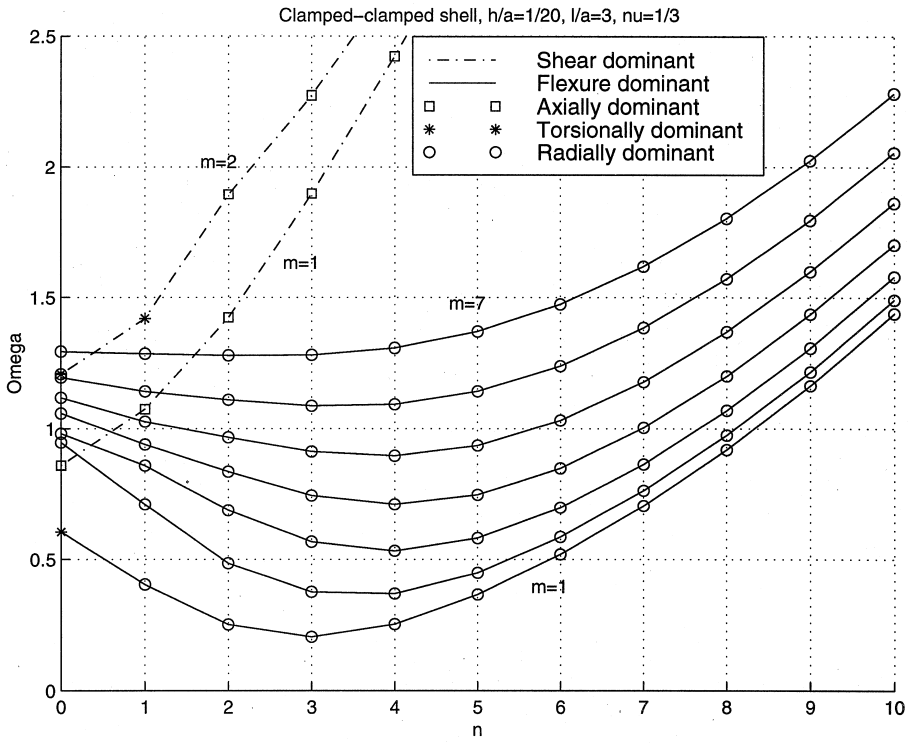

Fig. 12. Nondimensional frequency Ω vs mode numbers m and n for a clamped–clamped shell with $l/a = 3$, $h/a = 1/20$, and $\nu = 1/3$.

and dilatation dominated motion becomes superior. In fact, modes that begin as axial dominated motion at $n = 0$ evolve into predominantly torsional modes at larger n, and vice versa. In this and future cases, it was found that the first axisymmetric torsional mode begins the family of fundamental ($m = 1$) flexurally dominated modes. Discussion for other boundary conditions will be restricted to the flexural modes, as they make up the lowest set of frequencies. For comparison purposes, however, the first two shear mode curves will be shown as well, illustrating just how quickly they grow relative to the flexural behavior.

Since a clamped end or a free end represent the two possible extremes for a boundary condition, frequency behavior involving these two combinations will be addressed next. Figure 12 shows the clamped–clamped frequency behavior with increasing circumferential mode number n for a given axial mode number m. Figures 13 and 14 do so for clamped–free and free–free conditions, respectively. As mentioned earlier, although the axisymmetric torsional modes decouple from other mode types, they are still present and therefore must be accounted for when predicting shell frequencies. For each of the figures shown, modes with $n = 3$ or $n = 4$ tend to have the lowest frequencies for a given axial wave number.

To obtain an overall effect of boundary conditions on the shell flexural frequencies, Figs 12–14 can be examined together. Looking at them in the order 12, 13, and 14, the effect of changing a clamped end to a free end is an increase in the frequency band for small n while it decreases as n

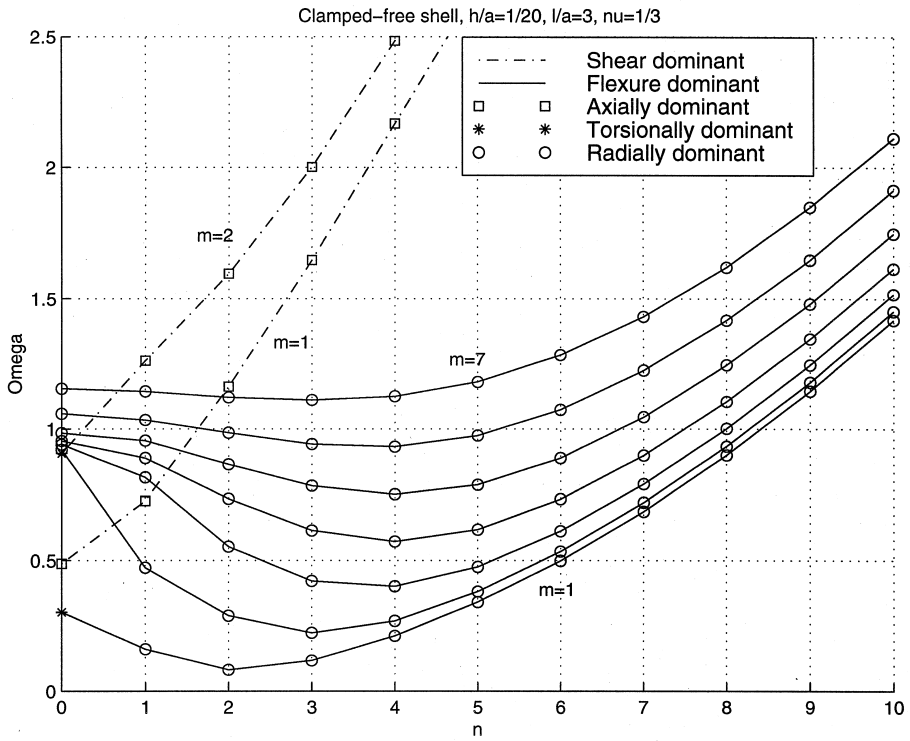

Fig. 13. Nondimensional frequency Ω vs mode numbers m and n for a clamped–free shell with $l/a = 3$, $h/a = 1/20$, and $\nu = 1/3$.

gets large. There is a tighter packing of the frequency bands at larger n as each fixed end gets released. Although only the first two shear modes are shown in each figure, a decrease in natural frequency and packing of these curves occurs as well.

For all the thin shell cases considered, none of the experimental work contained data for the axisymmetric ($n = 0$) modes. Although not directly stated in the references, there are several reasons why these modes may have been avoided. First of all, many of the experiments relied on the presence of nodal lines for resonance identification. For the axisymmetric torsional frequencies, there are no nodal lines using a small deflection approximation. Unless lines parallel to the longitudinal axis are drawn on the shell, motion of this type cannot be observed visually. Furthermore, most vibration sensors, such as accelerometers or piezoelectric films, rely on transverse bending for motion detection. This does not occur for pure torsion. Thus, the first detectable axisymmetric mode is often of the flexural type. Referring to Figs 12–14, there are 32, 35, and 44 other flexural frequencies present below the first axisymmetric flexural mode. Therefore, when checking for the shell modes using conventional measurement techniques, one will encounter a large number of natural modes before the first detectable axisymmetric mode is reached. These observations may explain why modes with $n = 0$ were not included in the experimental references. In addition, some experimental work cited here excluded frequency data for the bending modes ($n = 1$) as well. Referring to Figs 11–14, for $n \geqslant 2$, the first seven flexural modes appear well below

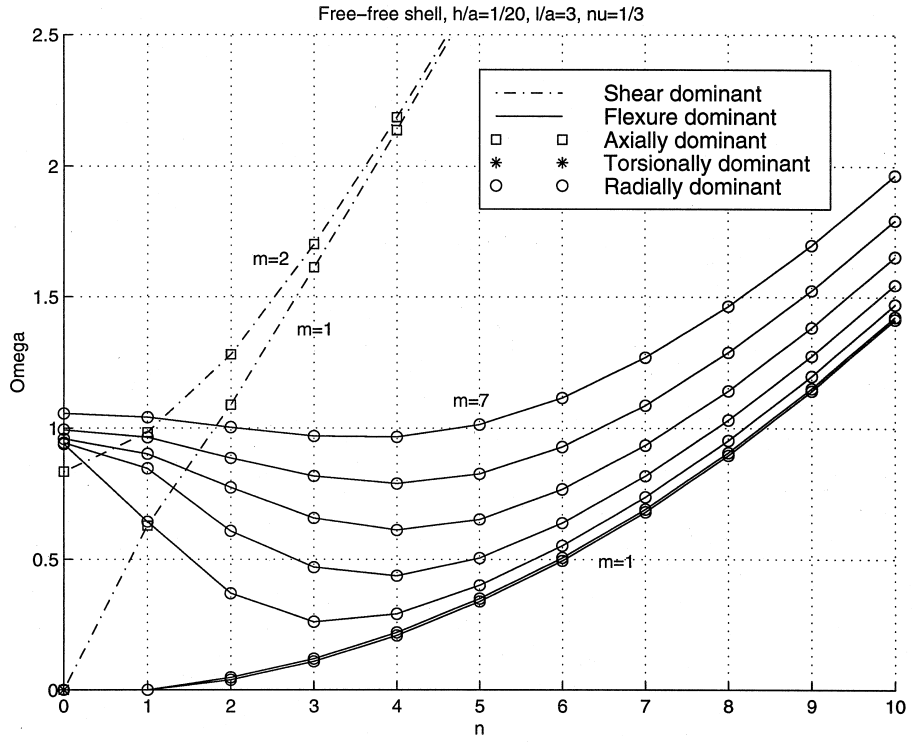

Fig. 14. Nondimensional frequency Ω vs mode numbers m and n for a free–free shell with $l/a = 3$, $h/a = 1/20$, and $\nu = 1/3$.

the first shear mode. Thus, one is assured the first seven modes will be flexurally dominant at higher values of n. Since most measurement techniques relied on appreciable bending deformation, the flexural modes will produce the strongest output signals.

Next, consider the effect of changing the length of the shell. This comparison will be done using clamped–free end conditions. Figure 13 showed the frequency behavior with increasing circumferential mode number n for a given axial number m. Figure 15 uses the same shell parameters except l/a is doubled. Using some intuition from beam vibration theory, the frequencies can be expected to decrease for a given (m, n) pair with an increase in axial length. Referring to Figs 13 and 15, this is indeed the case for small values of n. At large values of n, however, although the frequency band between $1 \leqslant m \leqslant 7$ is significantly decreased, the fundamental axial frequencies ($m = 1$) seem to approach the same values.

Upon further investigation of the Figs 11–15, note that they have the same behavior for the $m = 1$ flexural modes as n gets large, regardless of boundary conditions or length to radius ratios. Calladine (1983) derived a frequency equation for the bending modes of a simple ring. For a ring with rectangular cross-section, radius a, and radial thickness h, this result can be expressed in terms of the shell parameters defined earlier as:

$$\Omega = \beta n \frac{n^2 - 1}{\sqrt{n^2 + 1}} \tag{56}$$

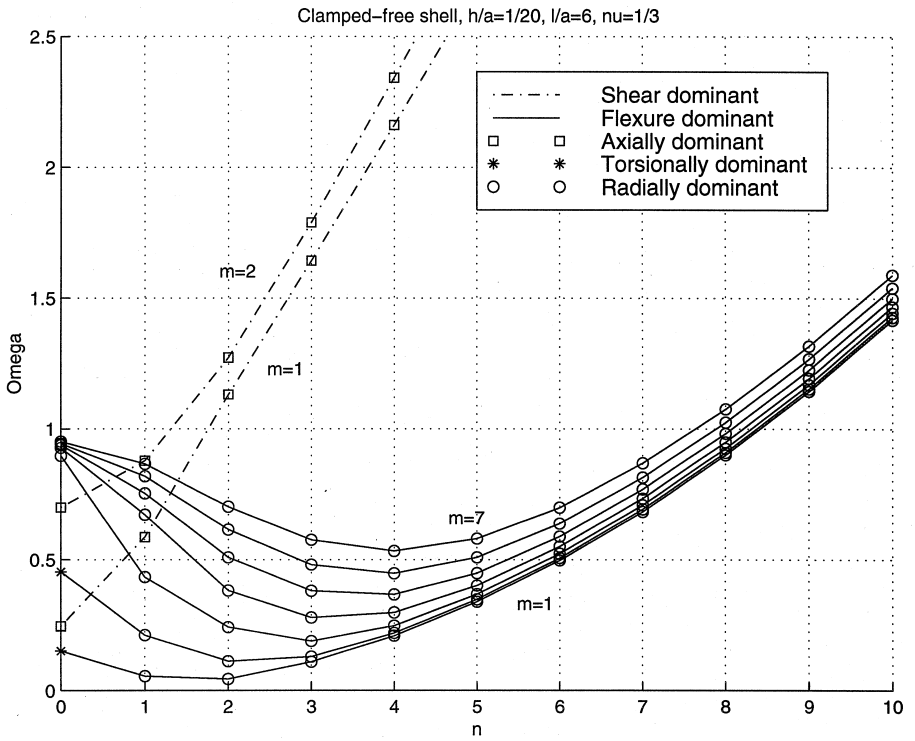

Fig. 15. Nondimensional frequency Ω vs mode numbers m and n for a clamped–free shell with $l/a = 6$, $h/a = 1/20$, and $v = 1/3$.

For the moment, assume that the cylindrical shell behaves like a ring when $m = 1$. Figure 16 shows the comparison of eqn (56) against the fundamental axial frequencies shown in Figs 11–15. As n gets large, the flexural frequencies converge to the same values, behaving as a ring in pure radial vibration. Thus, the hoop approximation acts as a lower bound on the fundamental axial modes. Note that this bound is independent of the boundary conditions or changes in shell length. This is the well-known result obtained by Rayleigh for the natural frequencies of an infinite cylindrical shell.

When searching for natural frequencies using the present approach, the MATLAB code needs a range of frequencies through which it will search. As shown through the experimental comparisons, Soedel's eqn (55) gave frequencies that were consistently higher than realized. Hence, we can use this equation as an upper bound for a given pair of n and m. For any set of boundary conditions and a given circumferential mode number, the frequency search can be started at the value given by eqn (56). If we want to find the first m axial modes for the chosen value of n, we increase Ω up to the value predicted by eqn (55), since the actual value for the mth frequency will be less than this bound. Soedel's equation together and the infinitely-long vibrating cylinder approximation serve as suitable bounds for the frequency search. This offers a significant reduction in computation time over a completely exhaustive eigenvalue search.

Now that the classical free and clamped ends have been examined, one can consider the effect

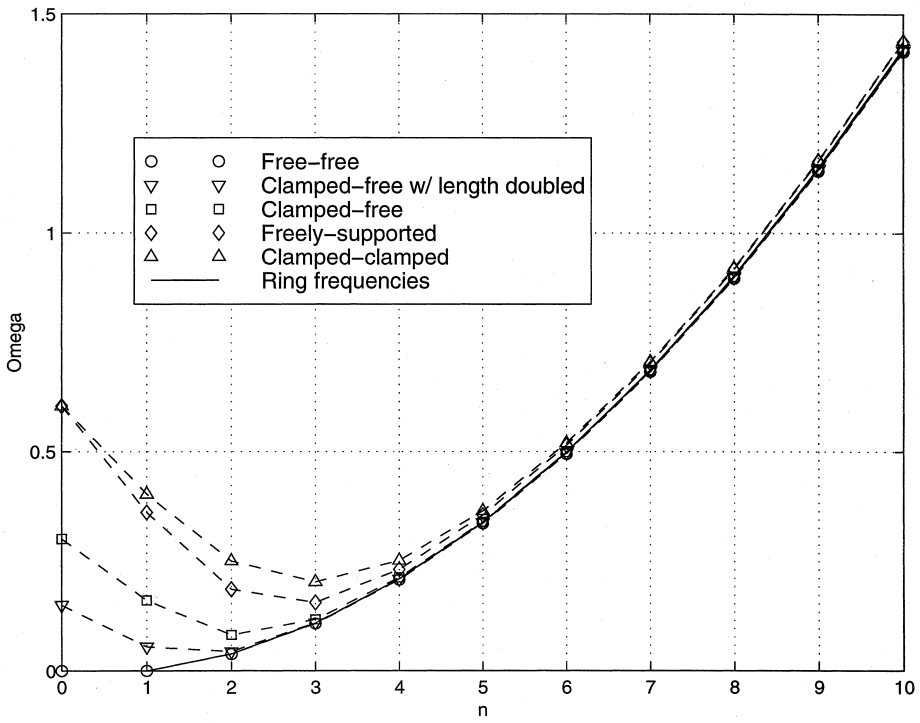

Fig. 16. Fundamental axial frequencies vs circumferential mode number n for the boundary conditions investigated.

of attaching a ring stiffener to a free end. Both the free end and the clamped end can be recovered from the elastic ring end condition by letting the ring properties take on extreme values. A rigid ring will be discussed first, attached to the clamped–free shell discussed earlier. In addition to ratios $\nu = 1/3$, $h/a = 1/20$, and $l/a = 3$, the ring has a rectangular cross-section with radial and longitudinal thickness ratios of $h_R/h = 5$ and $t_R/l = 0.01$. Clamped–clamped behavior for very large ρ_R/ρ values can be intuitively expected, with 'almost' clamped–free frequencies when ρ_R/ρ goes to zero. The latter will be due to the geometric constraints defined by eqns (41) and (42) that still remain, leading to frequencies slightly higher than the associated clamped–free values. Figures 17 and 18 show the behavior of the bending and axisymmetric modal frequencies as the ring density ratio is varied from $0 \leqslant \rho_R/\rho \leqslant 10^5$, where pure torsional motion is designated with dashed lines. These results were generated using the Q matrix entries for a clamped end in Table 2 at $z = 0$ and those for a rigid ring in Tables 4 and 5 at $z = l/a$. At very small values of ρ_R/ρ, the difference between the actual frequencies and clamped–free behavior grows with axial mode number m as a result of the two geometric constraints. For large ρ_R/ρ, however, the frequencies of the first two modes collapse to zero in both figures, denoted by question marks. As discussed earlier, the z-dependent rigid body motion of a shell consists of two axisymmetric modes and two in bending. These four frequencies get forced to zero as clamped–clamped end conditions are achieved. Each of these correspond to the rigid body modes of a massive ring. Thus, the question marks in Figs 17 and 18 are not mysterious at all, since the elastic strain energy is made up of both that of the

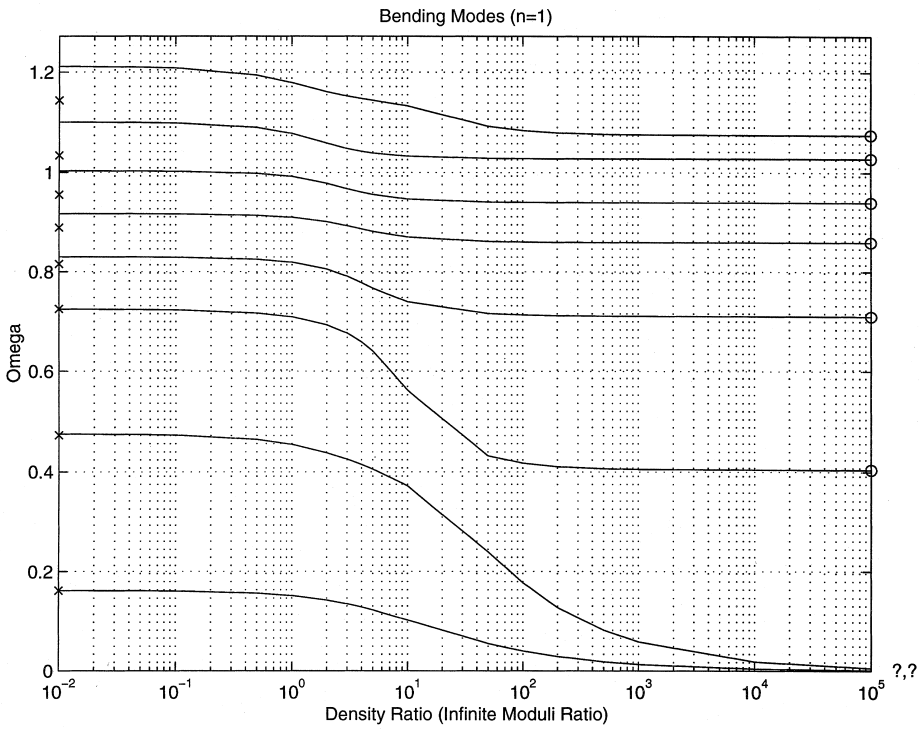

Fig. 17. Nondimensional frequency Ω vs ρ_R/ρ for the bending modes with a rigid ring stiffener, where (—) denotes actual data, (○) are the clamped–clamped values, and (×) are the clamped–free values.

shell and that of the ring stiffener. The behavior of the ring and the shell decouple in these extreme cases.

If we relax the rigid ring constraint by also permitting the ratio E_R/E to go to zero, we should recover the clamped–free frequencies of the shell discussed earlier, while retaining the clamped–clamped behavior at a large values of E_R/E and ρ_R/ρ. Figures 19 and 20 show the frequency evolution for the bending and axisymmetric modes with $E_R/E = \rho_R/\rho$ given the same shell and ring dimensions in Figs 17 and 18. These results were generated using the Q matrix entries for a clamped end in Table 2 at $z = 0$ and those for an elastic ring in Table 3 at $z = l/a$. When the ratio goes to zero, the clamped–free behavior is indeed recovered. At large values of $E_R/E = \rho_R/\rho$, however, four of the modes converged to frequencies (denoted by question marks) that were not predicted by the clamped–clamped eigensolution in both cases. These are modes for which the elastic ring is effectively vibrating as if the shell were not there. Thus, they need to be analyzed with the help of thin ring vibration theory.

The vibration problem of a thin elastic ring has been discussed by Love (1944) for circular cross-sections and extended to the rectangular case by Charnley et al. (1989). Four types of motion can exist for a vibrating circular ring. The first two are inextensional and extensional vibration and are called planar motion, for which the frequency of the latter is the larger of the pair. These can be interpreted as shapes where the mean circumference of the ring is and is not conserved during the

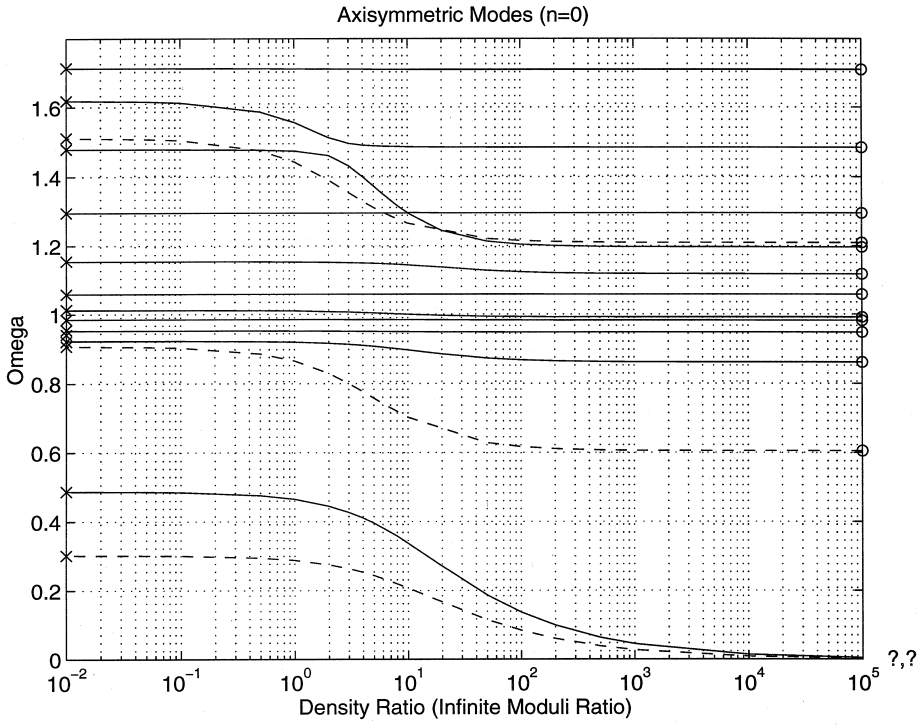

Fig. 18. Nondimensional frequency Ω vs ρ_R/ρ for the axisymmetric modes with a rigid ring stiffener, where (—) denotes actual data, (- -) denotes torsional data, (○) are the clamped–clamped values, and (×) are the clamped–free values.

motion. For further discussion on the nature of the ring mode shapes, the interested reader is referred to the original paper. Using the quantities defined throughout this paper, these frequencies satisfy the characteristic equation:

$$\Omega_{\text{inext,ext}}: \quad K_1\Omega^4 - K_2\Omega^2 + K_3 = 0, \quad \text{with the coefficients}$$

$$K_1 = \left[\frac{\rho_R/\rho}{(1-\nu^2)E_R/E}\right]^2 \left[\frac{A_R}{a^2} + (n^2+1)\frac{I^z}{a^4}\right]$$

$$K_2 = \frac{\rho_R/\rho}{(1-\nu^2)E_R/E}\left[(n^2+1)\frac{A_R}{a^2} + (2n^4-n^2+1)\frac{I^z}{a^4}\right]$$

$$K_3 = n^2(n^2-1)^2\frac{I^z}{a^4} \tag{57}$$

The other class is termed non-planar motion and consists of axial and torsional vibration, the latter type having the larger frequency. Although more difficult to envision than the previous class for higher values of n, the axial direction is along the θ-axis of the shell while torsion is oriented

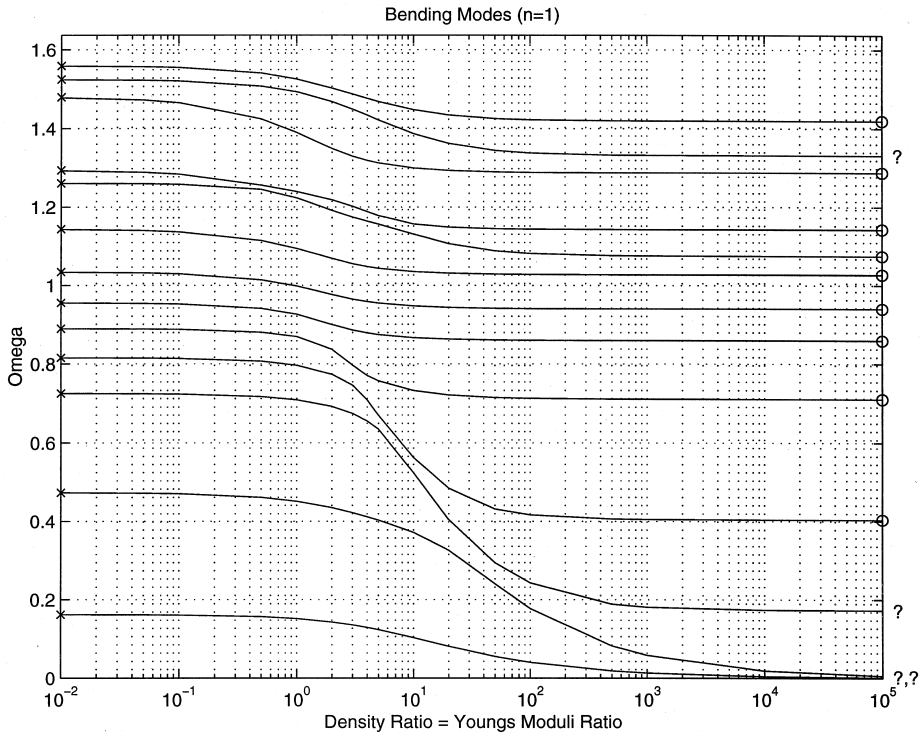

Fig. 19. Nondimensional frequency Ω vs $\rho_R/\rho = E_R/E$ for the bending modes with an elastic ring stiffener, where (—) denotes actual data, (○) are the clamped–clamped values, and (×) are the clamped–free values.

about the θ-axis. For an isotropic material, these frequencies arise from the following characteristic equation:

$$\Omega_{\text{axial,tors}}: \quad K_4\Omega^4 - K_5\Omega^2 + K_6 = 0, \quad \text{with the coefficients}$$

$$K_4 = \left[\frac{\rho_R/\rho}{(1-\nu^2)E_R/E}\right]^2 \frac{I^\theta}{a^4}\left(\frac{A_R}{a^2} + n^2\frac{I^r}{a^4}\right)$$

$$K_5 = \frac{\rho_R/\rho}{(1-\nu^2)E_R/E}\left\{\left[\frac{A_R}{a^2} + n^2\frac{I^r}{a^4}\right]\left[\frac{I^r}{a^4} + n^2\frac{C_T/a^4}{2(1+\nu_R)}\right] + n^2\frac{I^\theta}{a^4}\left[n^2\frac{I^r}{a^4} + \frac{C_T/a^4}{2(1+\nu_R)}\right]\right\}$$

$$K_6 = n^2(n^2-1)^2\frac{I^r}{a^4}\frac{C_T/a^4}{2(1+\nu_R)} \tag{58}$$

Using the present ring and shell dimensions, the changes in frequency parameter Ω for these four types vs n are shown in Fig. 21.

Each of the four terms appearing in the ring elastic strain energy (26) corresponds to one of the four independent ring modes mentioned here when both the density and Young's modulus are much larger than those of the shell itself. Thus, four of the shell frequencies will evolve into those

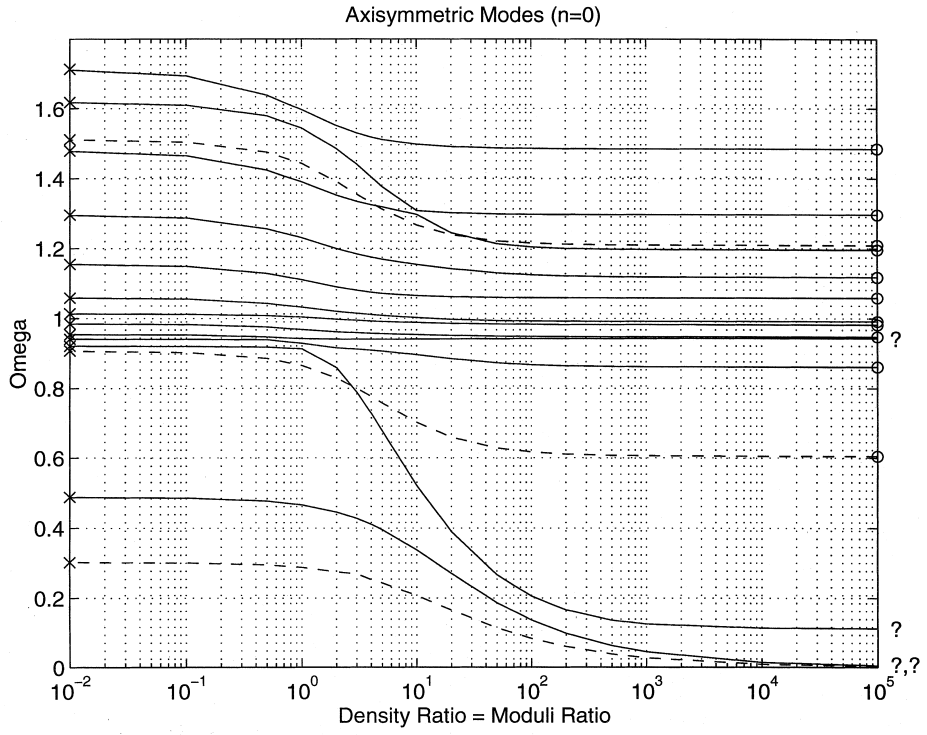

Fig. 20. Nondimensional frequency Ω vs $\rho_R/\rho = E_R/E$ for the axisymmetric modes with an elastic ring stiffener, where (—) denotes actual data, (- -) denotes torsional data, ($\bigcirc$) are the clamped–clamped values, and ($\times$) are the clamped–free values.

for a ring vibrating on its own, explaining the behavior observed in Figs 19 and 20. Looking at the frequency comparisons in Table 8, the four unknown frequencies in both cases have been identified when pure ring vibration is taken into account. According to Fig. 20, note that the second torsional mode for the clamped–free conditions becomes the first torsional mode for the

Table 8
Comparison of unexpected shell frequencies with those of pure ring behavior

Mode type	For the parameters	At large values of	Unexpected values for Ω	Vibrating ring (Fig. 21)			
				Ω_{axial}	Ω_{tors}	Ω_{inext}	Ω_{ext}
Bending (Fig. 19)	$t_R/l = 0.01$, $h_R/h = 5$	$\rho_R/\rho = E_R/E = 10^5$	0.0013, 0.0059, 0.1727, 1.332	0 (RBM)	0.1727	0 (RBM)	1.3316
Axisymmetric (Fig. 20)	$t_R/l = 0.01$, $h_R/h = 5$	$\rho_R/\rho = E_R/E = 10^5$	0.0027 (T), 0.0045, 0.1125, 0.9428	0 (RBM)	0.1123	0 (RBM)	0.9453

(T) denotes torsional axisymmetric modes. (RBM) denotes rigid body modes.

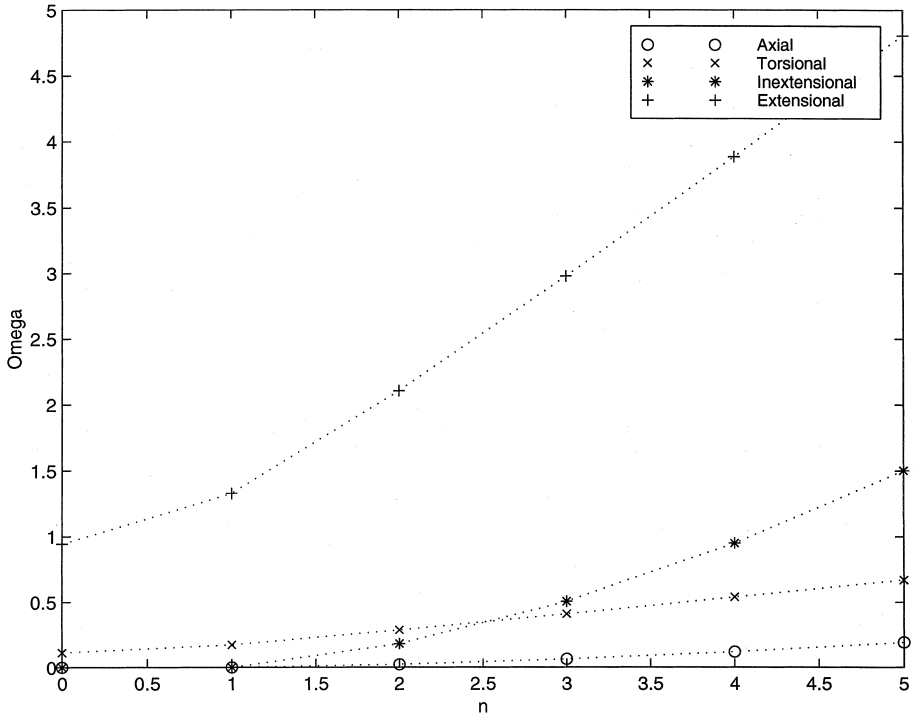

Fig. 21. Nondimensional frequency Ω vs n for the four ring vibration types.

clamped–clamped case (third becomes the second, etc.). This occurs because the first torsional frequency with the clamped–free ends evolves into a ring rigid body mode, producing trivial shell displacements.

For the axisymmetric extensional ring mode, there is a slight discrepancy between the frequency values. Following the ring theory of Charnley et al. and the present dimensionless quantities, the frequency for this mode is $\Omega = \sqrt{1-\nu^2} = 0.9428$. Using the ring energy expression (26), its value can be shown to be $\Omega = \sqrt{(1-\nu^2)(1+I_G^z/A_R a^2)} = 0.9453$. The second term in the additional factor under the radical is often negligible compared to unity, but has a small contribution here, making the frequency value about 0.3% higher.

If ρ_R and E_R are significantly larger than those of the shell, this does not imply that the ring is rigid. Rather, the dynamic behavior of the shell and the ring become independent sets of mode shapes in this case. Thus, four extra modes exist for each circumferential mode number n, in addition to those predicted by clamped–clamped behavior, due to a large but finite ring stiffness. At these frequencies, the ring vibrates as if the shell were not there at all. Using the non-dimensional parameters defined here, their values can be shown to be proportional to $\sqrt{(E_R/E)/(\rho_R/\rho)}$. The shell mode shapes corresponding to these frequencies show how the ring motion propagates through the shell to the other boundary. As an example, Fig. 22 shows how the mode corresponding to Ω_{04} evolves with increasing $E_R/E = \rho_R/\rho$. These are associated with the second lowest solid line in Fig. 20 which becomes the ring torsional mode as $E_R/E = \rho_R/\rho$ gets very large.

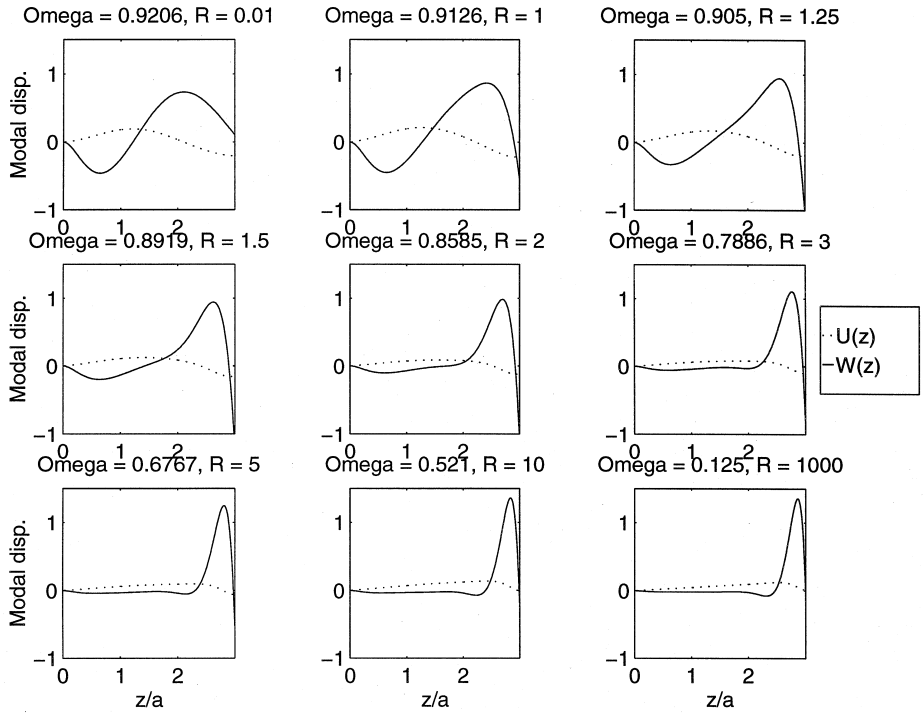

Fig. 22. Evolution of the fourth axisymmetric mode ($R = E_R/E = \rho_R/\rho$) from clamped–free behavior ($R = 0, \Omega_{04} = 0.9206$) to ring-dominated torsional vibration ($R \to \infty, \Omega_{0,\text{tors}} = 0.1123$).

Another study that the present solution procedure makes possible is the effect of ring eccentricity on the eigensolution. Here, the mean radii of the shell and ring were assumed to coincide, but ring eccentricity can be considered by substituting a_R for a everywhere it appears in the ring forces and defining the geometric relations between the ring and shell displacements. Although this complicates the expressions, it is a task that MAPLE can handle. As far as the MATLAB code is concerned, its sole purpose is number crunching leaving the Q matrix definitions to MAPLE. As long as the relevant shell parameters are given numerical values as they are introduced, the origin of the matrix entries is immaterial, further illustrating the flexibility of using the two packages together.

9. Conclusions

Due to the advent of high performance computers and robust commercial software packages, the solution to the vibration problem of thin isotropic circular cylindrical shells can be done in closed form with numerically determined coefficients. Since these coefficients are constants for a given mode, quantities that involve spatial derivatives can be found explicitly. No error due to finite difference approximations is introduced. As long as the equations of motion are derived consistently with the internal loads, the natural modes will be mutually orthogonal for a large

variety of boundary conditions, including the rigid body modes when they exist. Excellent agreement between experimental data and Junger and Feit's theory is obtained via the present approach. The power of the present solution procedure comes from the flexibility of the MAPLE code to change boundary conditions and the ease with which one can vary both shell and ring properties within MATLAB.

Acknowledgements

This research was supported by the Federal Aviation Administration through the Center of Excellence for the Computational Modeling of Aircraft Structures (CMAS) at Rutgers University. The authors would like to thank Dr Peter Shyprykevich, their technical monitor, for his helpful comments and suggestions.

References

Al-Najafi, A.M.J., Warburton, G.B., 1970. Free vibration of ring-stiffened cylindrical shells. Journal of Sound and Vibration 13 (1), 9–25.

Arnold, R.N., Warburton, G.B., 1953. The flexural vibrations of thin cylinders. Proceedings of the Institution of Mechanical Engineers 167, 62–80.

Bert, C.W., Baker, J.L., Egle, D.M., 1969. Free vibrations of multilayer anisotropic cylindrical shells. Journal of Composite Materials 3, 480–499.

Bogner, F.K., Archer, R.R., 1965. On the orthogonality condition of axisymmetric vibration modes for shells of revolution. Journal of Applied Mechanics 32, 447–448.

Bray, F.M., Egle, D.M., 1970. An experimental investigation of the free vibration of thin cylindrical shells with discrete longitudinal stiffeners. Journal of Sound and Vibration 12 (2), 153–164.

Brogan, F., Forsberg, K., Smith, S., 1968. Experimental and analytical investigation of the dynamic behavior of a cylinder with a cutout. Proceedings of the 9th AIAA/ASME Structures, Structural Dynamics, and Materials Conference 68 (318), 1–13.

Calladine, C.R., 1983. Theory of Shell Structures. Cambridge University Press, New York.

Callahan, J., 1997. Cylindrical shell vibrations: closed-form analysis and measurement via piezoelectric films. Doctoral dissertation, Rutgers University, Piscataway, NJ.

Charnley, T., Perrin, R., Mohanan, V., Banu, H., 1989. Vibrations of thin rings of rectangular cross-section. Journal of Sound and Vibration 134 (3), 455–488.

Chung, H., 1981. Free vibration analysis of circular cylindrical shells. Journal of Sound and Vibration 74 (3), 331–350.

El Raheb, M., Babcock, C.D. Jr., 1981. Effect of elastic end rings on the eigenfrequencies of thin cylinders. Journal of Sound and Vibration 74 (1), 31–46.

Flügge, W., 1960. Stresses in Shells. Springer-Verlag, Berlin.

Forsberg, K., 1964. Influence of boundary conditions on the modal characteristics of thin cylindrical shells. AIAA Journal 2 (12), 2150–2157.

Galletly, G., 1955. On the in-vacuo vibrations of simply supported, ring-stiffened cylindrical shells. Proceedings of the 2nd U.S. Congress on Applied Mechanics, pp. 225–231.

Gill, P.A.T., 1972. Vibrations of clamped–free circular cylindrical shells. Journal of Sound and Vibration 25 (3), 501–503.

Greenberg, M.D., 1978. Foundations of Applied Mathematics. Prentice-Hall, Englewood Cliffs, NJ.

Inman, D.J., 1994. Engineering Vibration. Prentice-Hall, Englewood Cliffs, NJ.

Junger, M.C., Feit, D., 1972. Sound, Structures, and Their Interaction. MIT Press, Cambridge.

Khadakkar, A.G., Narayanan, R., Ravi Sankar, K., Iyer, N.R., Appa Rao, T.V.S.R., 1988. Free vibrations of a cylindrical shell by holographic interferometry. Journal of Sound and Vibration 121 (1), 169–180.

Koga, T., 1988. Effects of boundary conditions on the free vibrations of circular cylindrical shells. AIAA Journal 26 (11), 1387–1394.

Koval, L.R., Cranch, E.T., 1962. On the free vibrations of thin cylindrical shells subjected to an initial static torque. Proceedings of the 4th U.S. Congress on Applied Mechanics, 1, 107–117.

Leissa, A.W., 1973. Vibration of Shells. NASA SP-288.

Love, A.E.H., 1944. A Treatise on the Mathematical Theory of Elasticity. Dover Publications, New York.

Ludwig, A., Krieg, R., 1981. An analytical quasi-exact method for calculating eigenvibrations of thin circular cylindrical shells. Journal of Sound and Vibration 74 (2), 155–174.

Meirovitch, L., 1967. Analytical Methods in Vibrations. Macmillan, New York.

Niordson, F., 1985. Shell Theory. Elsevier Science, New York.

Raj, D.M., Narayanan, R., Khaddakar, A.G., Paramasivam, V., 1995. Effect of ring stiffeners on vibration of cylindrical and conical shell models. Journal of Sound and Vibration 179 (3), 413–426.

Sharma, C.B., Johns, D.J., 1972. Natural frequencies of clamped–free circular cylindrical shells. Journal of Sound and Vibration 21 (3), 317–327.

Soedel, W., 1980. A new frequency formula for closed circular cylindrical shells for a large variety of boundary conditions. Journal of Sound and Vibration 70 (3), 309–317.

Soedel, W., 1981. Vibration of Shells and Plates. Marcel-Dekker, New York.

Tso, W.K., 1967. Orthogonality condition for the vibrational modes of elastic shells. Journal of Applied Mechanics 34, 782–784.

Vinson, J., 1974. Structural Mechanics: The Behavior of Plates and Shells. John Wiley and Sons, New York.

Warburton, G.B., 1965. Vibration of thin cylindrical shells. Journal of Mechanical Engineering Science 7 (4), 399–407.